

Review

## Unit quaternion description of spatial rotations in 3D electron cryo-microscopy



Mingxu Hu<sup>a,b,c,1</sup>, Qi Zhang<sup>d,1</sup>, Jing Yang<sup>d,\*</sup>, Xueming Li<sup>a,b,c,e,\*</sup>

<sup>a</sup> Key Laboratory of Protein Sciences (Tsinghua University), Ministry of Education, Beijing, China

<sup>b</sup> School of Life Science, Tsinghua University, Beijing, China

<sup>c</sup> Beijing Advanced Innovation Center for Structural Biology, China

<sup>d</sup> Department of Mathematical Sciences, Tsinghua University, China

<sup>e</sup> Beijing Frontier Research Center for Biological Structure, China

### A B S T R A C T

Electron cryo-microscopy (cryoEM) involves the estimation of spatial rotations, or saying orientations, of projection images or three-dimensional (3D) volumes. Euler angle system is widely used to describe spatial rotations in most cryoEM algorithms and software. In this review, we introduce unit quaternion as an alternate to Euler angles for describing spatial rotations, customize and develop corresponding tools for increasing demands of statistical analysis of spatial rotations in cryoEM. Some basic properties and definitions of quaternion are first recalled. Thereafter, distance and geodesic between rotations are introduced to aid comparisons and interpolations between rotations, which are prerequisites of statistics of rotations in 3D cryoEM. Furthermore, statistics of rotations are reviewed. Techniques potentially useful in cryoEM, such as calculations of the average rotation, generation of quasi-regular grids, sampling, inference with uniform distribution and angular central Gaussian (ACG) distribution, and estimation of rotation precision, are reviewed and developed. Finally, molecular symmetry presented in unit quaternion form is discussed. Unit quaternion system is shown as a convenient and comprehensive mathematical tool for cryoEM.

### 1. Introduction

In the three-dimensional (3D) reconstruction of electron cryo-microscopy (cryoEM), particle images or pre-reconstructed sub-tomograms of biological samples require rotation in 3D spaces to specific orientations for enabling the reconstruction of a 3D density map (Grant et al., 2018; Guang Tang et al., 2007; Joachim et al., 1981; Grigorieff, 2018; Punjani et al., 2017; Scheres, 2012; Shaikh Tanvir et al., 2008). Accordingly, the description, determination, operation, and analysis of rotations are important for cryoEM. Different algorithms have been developed to determine the parameters of rotation, i.e., orientation, to achieve a better rotation precision for higher resolution. Methods based on statistical analysis of rotations have been used in Mingxu et al. (2018) in the development of such algorithms.

To describe spatial rotations, the three approaches widely used in differing fields are rotation matrix, Euler angles, and unit quaternion. The rotation matrix is the most basic one, and can be directly used to rotate a 3D vector or object. However, nine parameters with non-linear constraints in a  $3 \times 3$  matrix are required to describe a 3D rotation that is often infeasible for algorithms to directly estimate and optimize. The Euler angle description is an alternative approach that parameterizes the rotation matrix using three angle values that represent sequential

rotations around three elemental axes. There are two definitions for Euler angles based on intrinsic rotations relative to the object space that changes after each rotation, and on extrinsic rotations relative to a fixed coordinate system, respectively. Each definition has six conventions of elemental axis sets, for example, the convention with Z, Y, and Z axes widely used in cryoEM. Euler angles are intuitive; hence, they have been adopted in cryoEM for beyond 40 years (Grant et al., 2018; Guang Tang et al., 2007; Joachim et al., 1981; Grigorieff, 2018; Punjani et al., 2017; Scheres, 2012; Shaikh Tanvir et al., 2008).

However, the Euler angle system has several drawbacks compared with the other two systems. One is the non-uniformity of rotation description that can cause orientation optimization in unexpected directions. Furthermore, the gimbal lock is a well-known problem of the Euler angles that occurs in the definition of intrinsic rotations and causes failure of optimization algorithm (see Appendix A). Moreover, owing to the existence of multiple definitions and axis conventions, the conversion of Euler angles from one program to another is often confusing. In addition, the statistical analysis of the Euler angles is predominantly difficult.

The unit quaternion is a different system from the rotation matrix and Euler angles, and addresses several drawbacks of Euler angles including those described. There have been attempts to adopt unit

\* Corresponding author at: School of Life Science, Tsinghua University, Beijing, China.

E-mail addresses: [y-j@tsinghua.edu.cn](mailto:y-j@tsinghua.edu.cn) (J. Yang), [liueming@tsinghua.edu.cn](mailto:liueming@tsinghua.edu.cn) (X. Li).

<sup>1</sup> These authors contributed equally to this work.

quaternion description in cryoEM. In 1990, Harauz (Harauz, 1990) stated that quaternion can be used in cryoEM because the absolute orientation problem is solvable by unit quaternion description in closed form (Berthold, 1987). Consequently, quaternion-assisted angular reconstitution approach (Farrow and Ottensmeyer, 1992; Farrow and Ottensmeyer, 1993) was developed. Several structures (Irina et al., 1995; Dube et al., 1995; Orlova and Van Heel, 1994; Orlova et al., 1996; Orlova et al., 1997; Schatz et al., 1995; Stark et al., 1995; Stark et al., 1997; Czarnota et al., 1994; Czarnota and Ottensmeyer, 1996; Bazett-Jones et al., 1996) were addressed by this approach at 10–30 Å resolution, reviewed by Schatz et al. (1997). Following the development of cryoEM image processing, multiple algorithms or packages have emerged. Several of them (Baldwin and Penczek, 2007; Frank et al., 1996; Guang Tang et al., 2007; Hrabe, 2015; Joachim et al., 1981; Kuo, 2007; Liu et al., 2007; Plaisier et al., 2007; Sommer and Brimacombe, 2001; Topf et al., 2008; Wasilewski and Rosenthal, 2014; Gydo and Alexandre, 2015; Pandurangan et al., 2015) adopted unit quaternion. The unit quaternion was used to perform basic rotations (Baldwin and Penczek, 2007; Frank et al., 1996; Guang Tang et al., 2007; Joachim et al., 1981; Kuo, 2007), generate uniform or quasi-uniform sampling in rotation space (Plaisier et al., 2007; Liu et al., 2007; Wasilewski and Rosenthal, 2014; Pandurangan et al., 2015; Gydo and Alexandre, 2015), and cooperate with model building (Sommer and Brimacombe, 2001; Liu et al., 2007; Topf et al., 2008; Pandurangan et al., 2015; Hrabe, 2015; Gydo and Alexandre, 2015).

This review aims to systematically introduce the unit quaternion in cryoEM (Herman and Frank, 2014), and highlight the properties in statistics of spatial rotations based on unit quaternion. Some were used for the statistical inference in the particle-filter algorithm of THUNDER (Mingxu et al., 2018). For completeness, Section 2 presents a brief recall of definitions and basic properties of the quaternion, and a method to use the unit quaternion to describe and perform rotations. In Section 3, the definitions of the distance and geodesic between two rotations for cryoEM are discussed. These are the prerequisites of the statistical analysis and corresponding development. In Section 4, several methods for uniform or quasi-uniform sampling of rotation space are reviewed. Furthermore, in Section 5, the statistical analysis methods in the rotational space of cryoEM are introduced and developed. Finally, in Section 6, the method of managing molecular symmetry and corresponding space division of asymmetric units are discussed.

## 2. Background of the quaternion and unit quaternion description

The quaternion and unit quaternion description of rotation is developed and applied in several fields. In these section, we recall some properties and features of the quaternion and unit quaternion that is suitable for cryoEM. For more general introductions, we refer to these references (Vince, 2011; Conway and Smith, 2003).

The following notations will be used in this review. 3D vector is denoted by a letter with a bold font and an arrow on hat, for example,  $\vec{v}$ . The corresponding unit vector is written with a triangle hat, for example,  $\hat{v}$ . The quaternion in vector form and a four-dimensional (4D) vector are denoted by a letter with a bold font, for example,  $\mathbf{q}$ . The spatial rotation operator is denoted by  $R$ . All vectors are presented as column matrices, and the superscript,  $T$ , indicates matrix transpose. Moreover, the 3D space is denoted by  $\mathbb{R}^3$ , and all unit 3D vectors form a 2D surface of a unit sphere denoted by  $S^2$  in 3D space. Similarly, the 4D space is denoted by  $\mathbb{R}^4$ , and all unit 4D vectors form a 3D hypersurface of the unit sphere denoted by  $S^3$  in 4D space. The set containing all 3D spatial rotations is denoted by  $SO(3)$ .

### 2.1. Definitions and basic properties of the quaternion

A quaternion is an extension of a complex number. A quaternion  $\mathbf{q}$  is defined as a hypercomplex number composed of a real part and three imaginary parts as

$$\mathbf{q} = q_0 + q_1 \mathbf{i} + q_2 \mathbf{j} + q_3 \mathbf{k}. \quad (1)$$

Equivalently, a quaternion is often written in 4D vector form as

$$\mathbf{q} = \begin{pmatrix} q_0 \\ q_1 \\ q_2 \\ q_3 \end{pmatrix} = \begin{pmatrix} q_0 \\ \vec{\mathbf{n}}_{\mathbf{q}} \end{pmatrix}, \quad (2)$$

where  $\{\mathbf{i}, \mathbf{j}, \mathbf{k}\}$  are three imaginary units, and  $\vec{\mathbf{n}}_{\mathbf{q}} = \begin{pmatrix} q_1 \\ q_2 \\ q_3 \end{pmatrix}$ .

The conjugate of a quaternion is defined by

$$\mathbf{q}^* = q_0 - q_1 \mathbf{i} - q_2 \mathbf{j} - q_3 \mathbf{k} = \begin{pmatrix} q_0 \\ -\vec{\mathbf{n}}_{\mathbf{q}} \end{pmatrix}. \quad (3)$$

The norm of a quaternion  $\mathbf{q}$  is defined by

$$|\mathbf{q}| := \sqrt{q_0^2 + q_1^2 + q_2^2 + q_3^2} = \sqrt{q_0^2 + \vec{\mathbf{n}}_{\mathbf{q}} \cdot \vec{\mathbf{n}}_{\mathbf{q}}}. \quad (4)$$

The multiplication of two quaternions,  $\mathbf{q}$  and  $\mathbf{q}'$ , is calculated based on the multiplication rule on the basis elements, 1,  $\mathbf{i}$ ,  $\mathbf{j}$ , and  $\mathbf{k}$  given by

$$\begin{aligned} 1 \otimes 1 &= 1, 1 \otimes \mathbf{i} = \mathbf{i} \otimes 1 = \mathbf{i}, \\ 1 \otimes \mathbf{j} &= \mathbf{j} \otimes 1 = \mathbf{j}, 1 \otimes \mathbf{k} = \mathbf{k} \otimes 1 = \mathbf{k}, \\ \mathbf{i}^2 &= \mathbf{j}^2 = \mathbf{k}^2 = -1, \\ \mathbf{i} \otimes \mathbf{j} &= \mathbf{k}, \mathbf{j} \otimes \mathbf{k} = \mathbf{i}, \mathbf{k} \otimes \mathbf{i} = \mathbf{j}, \\ \mathbf{j} \otimes \mathbf{i} &= -\mathbf{k}, \mathbf{k} \otimes \mathbf{j} = -\mathbf{i}, \mathbf{i} \otimes \mathbf{k} = -\mathbf{j}, \end{aligned} \quad (5)$$

where  $\otimes$  represents the quaternion product. The result of quaternion multiplication can also be written in vector form as

$$\begin{aligned} \mathbf{q} \otimes \mathbf{q}' &= \begin{pmatrix} q_0 \\ q_1 \\ q_2 \\ q_3 \end{pmatrix} \otimes \begin{pmatrix} q'_0 \\ q'_1 \\ q'_2 \\ q'_3 \end{pmatrix} = \begin{pmatrix} q_0 q'_0 - q_1 q'_1 - q_2 q'_2 - q_3 q'_3 \\ q_0 q'_1 + q_1 q'_0 + q_2 q'_3 - q_3 q'_2 \\ q_0 q'_2 - q_1 q'_3 + q_2 q'_0 + q_3 q'_1 \\ q_0 q'_3 + q_1 q'_2 - q_2 q'_1 + q_3 q'_0 \end{pmatrix} \\ &= \begin{pmatrix} q_0 \\ \vec{\mathbf{n}}_{\mathbf{q}} \end{pmatrix} \otimes \begin{pmatrix} q'_0 \\ \vec{\mathbf{n}}_{\mathbf{q}'} \end{pmatrix} = \begin{pmatrix} q_0 q'_0 - \vec{\mathbf{n}}_{\mathbf{q}} \cdot \vec{\mathbf{n}}_{\mathbf{q}'} \\ q_0 \vec{\mathbf{n}}_{\mathbf{q}'} + q'_0 \vec{\mathbf{n}}_{\mathbf{q}} + \vec{\mathbf{n}}_{\mathbf{q}} \times \vec{\mathbf{n}}_{\mathbf{q}'} \end{pmatrix}, \end{aligned} \quad (6)$$

where  $\cdot$  and  $\times$  represent the inner product and cross product of vectors. The complex form and vector form of quaternion multiplication are equivalent. For simplicity, the vector form of a quaternion will be frequently used herein. Further basic properties of quaternion algebra are discussed in Appendix B.

### 2.2. Unit quaternion description of three-dimensional spatial rotation

If norm equals to 1, i.e.,  $|\mathbf{q}| = 1$ , then the quaternion  $\mathbf{q}$  is called a unit quaternion. The product of a unit quaternion  $\mathbf{q}$  with its conjugate is 1, because  $\mathbf{q} \otimes \mathbf{q}^* = \mathbf{q}^* \otimes \mathbf{q} = (1, 0, 0, 0)^T$ ; all unit quaternions form  $S^3$  (see Appendix B for more properties). A unit quaternion can be used to perform 3D rotation. A brief introduction is as follows.

The rotation of a 3D vector  $\vec{v}$  to another vector  $\vec{v}'$  is performed using a  $3 \times 3$  orthogonal matrix  $\mathbf{M}$  with a determinant of 1, as follows.

$$\vec{v}' = \mathbf{M} \vec{v}. \quad (7)$$

This operation can also be achieved by performing unit quaternion multiplication. Considering  $\vec{v}$  as  $\mathbf{v} = \begin{pmatrix} 0 \\ \vec{v} \end{pmatrix}$  in quaternion form, the rotation operation induced by unit quaternion  $\mathbf{q}$  is defined by Vince (2011)

$$\mathbf{v}' = \begin{pmatrix} 0 \\ \vec{v}' \end{pmatrix} = \mathbf{q} \otimes \begin{pmatrix} 0 \\ \vec{v} \end{pmatrix} \otimes \mathbf{q}^*. \quad (8)$$

In the following context, we will not distinguish between  $\mathbf{v}$  and  $\begin{pmatrix} 0 \\ \vec{v} \end{pmatrix}$ . For simplicity,  $R_{\mathbf{q}}$  is used to represent a rotation by unit quaternion  $\mathbf{q}$ , i.e.,

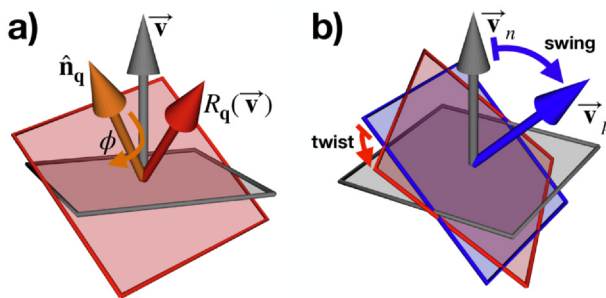


**Fig. 1. Rotations and swing-twist decomposition of the unit quaternion.** **a,** A unit quaternion  $\left(\cos\frac{\phi}{2}, \hat{n}_q \sin\frac{\phi}{2}\right)^T$  stands for a rotation around axis  $\hat{n}_q$  (orange) for rotation angle  $\phi$ , which rotates ( $R_q(\vec{v})$ ) a grey rectangle with norm vector of  $\vec{v}$  to the red one. **b,** Rotation from the grey rectangle to the red one is decomposed into two steps by swing-twist decomposition. In the swing step, the grey rectangle with norm vector  $\vec{v}_n$  is rotated to the blue rectangle with norm vector  $\vec{v}_p$  around the axis perpendicular to  $\vec{v}_n$  and  $\vec{v}_p$ . Then, the blue rectangle is further twisted around axis  $\vec{v}_p$  to the position of the red rectangle.

$$R_q(\vec{v}) = \mathbf{q} \otimes \begin{pmatrix} 0 \\ \vec{v} \end{pmatrix} \otimes \mathbf{q}^*. \quad (9)$$

Note that a pair of unit quaternions is involved in the multiplication; hence,  $\mathbf{q}$  and  $-\mathbf{q}$  will not yield different rotations (Vince, 2011). Consequently,  $R_q = R_{-\mathbf{q}}$ .

A unit quaternion explicitly represents a 3D spatial rotation about an axis. A unit quaternion  $\mathbf{q}$  can be written in the form (Conway and Smith, 2003)

$$\begin{pmatrix} \cos\frac{\phi}{2} \\ \hat{n}_q \sin\frac{\phi}{2} \end{pmatrix} \quad (10)$$

that describes a rotation about the axis  $\hat{n}_q$  by the angle  $\phi$  (Fig. 1a).

For sequential rotations, such as  $R_{\mathbf{q}_1}$  followed by  $R_{\mathbf{q}_2}$ , the unit quaternion of the overall rotation is calculated as (Vince 2011)

$$\begin{aligned} R_{\mathbf{q}_2}(R_{\mathbf{q}_1}(\vec{v})) &= \mathbf{q}_2 \otimes \left( \mathbf{q}_1 \otimes \begin{pmatrix} 0 \\ \vec{v} \end{pmatrix} \otimes \mathbf{q}_1^* \right) \otimes \mathbf{q}_2 \\ &= (\mathbf{q}_2 \otimes \mathbf{q}_1) \otimes \begin{pmatrix} 0 \\ \vec{v} \end{pmatrix} \otimes (\mathbf{q}_2 \otimes \mathbf{q}_1)^* \\ &= R_{\mathbf{q}_2 \otimes \mathbf{q}_1}(\vec{v}) \end{aligned} \quad (11)$$

demonstrating that  $\mathbf{q}_2 \otimes \mathbf{q}_1$  represents the overall rotation. Moreover, the dot and cross products of vectors are preserved under spatial rotations, i.e., quaternion multiplications (Winitzki, 2010). This is useful for combined computations of quaternion multiplication and vector multiplication.

Finally, the conversions between three rotation descriptions, namely the rotation matrix, Euler angles, and unit quaternion description, are well-established. The formulas of these conversions are summarized in Appendices C and D.

### 2.3. Swing-twist decomposition

If using a directional vector to represent the orientation of a 3D object, the 3D rotation of this object can be decomposed into the product of two rotations, a swing that changes the directional vector to another direction and a twist about the directional vector called swing-twist decomposition (Dobrowolski, 2015). This can be useful for rotation analysis and the application of constraints to rotations.

To demonstrate the potential application of the swing-twist decomposition in cryoEM, we consider a 2D experimental image in single-particle cryoEM that is rotated using unit quaternion  $\mathbf{q}$  to match the projection of a 3D object. In cryoEM, we assume that the experimental

image initially lies in the XY-plane with norm vector  $\vec{v}_n = (0, 0, 1)^T$ . The rotation can be performed in two steps (Fig. 1b).

First, the image is rotated so that its norm vector  $\vec{v}_n$  is changed to be along the projection direction  $\vec{v}_p$  called the swing.  $\vec{v}_p$  is calculated as follows.

$$\begin{pmatrix} 0 \\ \vec{v}_p \end{pmatrix} = \mathbf{q} \otimes \begin{pmatrix} 0 \\ \vec{v}_n \end{pmatrix} \otimes \mathbf{q}^*. \quad (12)$$

The swing rotating  $\vec{v}_n$  to  $\vec{v}_p$  can be obtained by a rotation about the axis

$$\hat{\mathbf{v}}_r = \frac{\vec{v}_n \times \vec{v}_p}{|\vec{v}_n| |\vec{v}_p|} \quad (13)$$

for the angle

$$\psi_s = \cos^{-1} \frac{\vec{v}_n \cdot \vec{v}_p}{|\vec{v}_n| |\vec{v}_p|}, \quad (14)$$

called the swing angle. Accordingly, the swing quaternion is

$$\mathbf{q}_s = \begin{pmatrix} \cos\frac{\psi_s}{2} \\ \hat{\mathbf{v}}_r \sin\frac{\psi_s}{2} \end{pmatrix}. \quad (15)$$

Second, the image is in-plane rotated about its norm vector; currently,  $\vec{v}_p$ , for angle  $\psi_t$  to match the projection of the object, called the twist. The twist quaternion is

$$\mathbf{q}_t = \begin{pmatrix} \cos\frac{\psi_t}{2} \\ \vec{v}_p \sin\frac{\psi_t}{2} \end{pmatrix} \quad (16)$$

as  $\vec{v}_p$  is a unit vector.

From the definition of swing-twist decomposition, i.e.,  $\mathbf{q} = \mathbf{q}_t \otimes \mathbf{q}_s$ , the twist quaternion  $\mathbf{q}_t = \mathbf{q} \otimes \mathbf{q}_s^*$  can be calculated. By comparing  $\mathbf{q}_t$  with Eq. (16), the twist angle  $\psi_t$  can be calculated.

The decomposing  $\mathbf{q} = \mathbf{q}_t \otimes \mathbf{q}_s$  mentioned above is known as the swing-before-twist form. The swing-twist decomposition also has a twist-before-swing form, wherein the twist is performed before the swing. Because  $\mathbf{q}^{-1} = \mathbf{q}^* = \mathbf{q}_s^* \otimes \mathbf{q}_t^* = \mathbf{q}_s^{-1} \otimes \mathbf{q}_t^{-1}$ , the twist-before-swing form can also be considered as the inversion of the swing-before-twist form.

### 3. Distance and geodesic between rotations by unit quaternion in cryoEM

In cryoEM, it is important to examine the differences between rotation parameters. However, there are no quantitative measure for such differences in cryoEM. Herein, we used the concept of distance between two rotations based on the unit quaternion system as a quantitative measure.

In particular, the definition of distance is a prerequisite of directional statistics in 3D rotational space  $SO(3)$  that aids statistical analysis, i.e., sampling and inference, in the rotation parameter space (discussed in the following sections). In some cryoEM programs, such as RELION (Scheres, 2012) and cryoSPARC (Punjani et al., 2017), HEALPix (Gurski et al., 2005) grid distance under constrained conditions with the Euler angle system is used as an approximate measure for the differences of rotation parameters. However, the properties of Euler angles limit the application of the rotation distance. In contrast, the definition of the distance and corresponding geodesic based on the unit quaternion has shown its advantages as a general mathematical tool for angular analysis and rotational operations.

#### 3.1. Definition of distance between rotations

The angle between two 3D unit vectors  $\vec{v}_1$  and  $\vec{v}_2$  can be defined

using the distance between them as follows.

$$d_{S^2}(\vec{v}_1, \vec{v}_2) := \cos^{-1}(\vec{v}_1 \cdot \vec{v}_2) \quad (17)$$

ranges  $[0, \pi]$ . Because  $\vec{v}_1$  and  $\vec{v}_2$  correspond to two points on the unit sphere  $S^2$ , the distance between  $\vec{v}_1$  and  $\vec{v}_2$  is the length of the shortest arc between their corresponding points on  $S^2$ . Using the angle value as the distance is straightforward for orientation analysis. However, the unit quaternion presents a rotation alternate to a 3D vector. Thus, the distance between two rotations is not explicit.

A comprehensible definition of the distance is useful to understand the physical meaning of a distance formula in cryoEM. Although there are several definitions of the distance between rotations in  $SO(3)$ , as summarized by Du (2009), insignificant attention have been received in cryoEM approaches. We raise the definition of distance between two rotations in  $SO(3)$ ,  $R_{\mathbf{q}_1}$  and  $R_{\mathbf{q}_2}$ , by

$$d_{SO(3)}(R_{\mathbf{q}_1}, R_{\mathbf{q}_2}) := \max_{\vec{v} \in S^2} d_{S^2}(R_{\mathbf{q}_1}(\vec{v}), R_{\mathbf{q}_2}(\vec{v})) \quad (18)$$

that is the maximum distance between two 3D vectors,  $R_{\mathbf{q}_1}(\vec{v})$  and  $R_{\mathbf{q}_2}(\vec{v})$ , generated by rotating an arbitrary unit vector  $\vec{v}$  using unit quaternion  $\mathbf{q}_1$  and  $\mathbf{q}_2$ . By abuse of notations, we denote  $d_{SO(3)}(R_{\mathbf{q}_1}, R_{\mathbf{q}_2})$  by  $d_{SO(3)}(\mathbf{q}_1, \mathbf{q}_2)$  in the following context. This definition satisfies the requirements of distance definition in mathematics (see Appendix E.1).

Accordingly, the distance can be calculated as (see Appendix E.2)

$$d_{SO(3)}(\mathbf{q}_1, \mathbf{q}_2) = 2\cos^{-1}(|\mathbf{q}_1 \cdot \mathbf{q}_2|). \quad (19)$$

This formula is the same as that used by Baldwin and Penczek (2007) in EMAN2 (Guang Tang et al., 2007). Plaisier et al. used the distance between two rotations  $R_{\mathbf{q}_1}$  and  $R_{\mathbf{q}_2}$  given by

$$2\cos^{-1}\left(1 - \frac{|\mathbf{q}_1 - \mathbf{q}_2|^2}{2}\right) \quad (20)$$

in Cyclops (Plaisier et al., 2007). Eq. (19) can be derived from Eq. (20) (see Appendix E.2), and, hence, are equivalent to each other.

From the definition of the distance,  $\cos^{-1}(|\mathbf{q}_1 \cdot \mathbf{q}_2|)$  in Eq. (19) is the shortest arc between  $\mathbf{q}_1$  and  $\mathbf{q}_2$  on the surface of sphere  $S^3$ . The coefficient 2 is a by-product of the fact that unit quaternion space  $S^3$  and rotation space  $SO(3)$  form a 2 – 1 homomorphism. The absolute value in the calculation of  $|\mathbf{q}_1 \cdot \mathbf{q}_2|$  indicates that  $\mathbf{q}_i$  and  $-\mathbf{q}_i$  ( $i = 1, 2$ ) represent the same rotation and will not yield different distances.

In the cryoEM scenario, the distance defined above provides an estimate of the possible maximal changes of projection directions from different rotations by

$$d_{SO(3)}(\mathbf{q}_1, \mathbf{q}_2) \geq d_{S^2}(\vec{v}_{p_{\mathbf{q}_1}}, \vec{v}_{p_{\mathbf{q}_2}}) \quad (21)$$

where  $\vec{v}_{p_{\mathbf{q}_1}}$  and  $\vec{v}_{p_{\mathbf{q}_2}}$  are the projection directions from rotations  $R_{\mathbf{q}_1}$  and  $R_{\mathbf{q}_2}$ , respectively (see Appendix E.3). For example, the rotation parameters of a particle image in single-particle cryoEM are updated for multiple rounds of 3D alignment. Measuring the distance of rotations between different rounds yields direct information on the convergence of 3D alignment.

### 3.2. Geodesic between rotations

In geometry, the geodesic is a curve or line indicating the shortest path between two points on a surface. Herein, we introduce the geodesic between two rotations,  $R_{\mathbf{q}_1}$  and  $R_{\mathbf{q}_2}$ , i.e., as the evolvement from the rotation  $R_{\mathbf{q}_1}$  to the rotation  $R_{\mathbf{q}_2}$  along the shortest path in  $SO(3)$ , which can be used for the interpolation between two rotations.

In the unit quaternion system, this geodesic is the shortest arc connecting the corresponding unit quaternions of rotations  $R_{\mathbf{q}_1}$  and  $R_{\mathbf{q}_2}$  on the surface  $S^3$  that is  $\cos^{-1}(|\mathbf{q}_1 \cdot \mathbf{q}_2|)$  as discussed earlier. From Eq. (19), the distances between  $\mathbf{q}_1$  and  $\mathbf{q}_2$ , and between  $\mathbf{q}_1$  and  $-\mathbf{q}_2$  are equal. However, the shortest arcs connecting  $\mathbf{q}_1$  and  $\mathbf{q}_2$ , and  $\mathbf{q}_1$  and  $-\mathbf{q}_2$  can have different lengths. Because the distance of corresponding

rotations is proportional to the shortest arc, the shortest is selected as the geodesic. Srivastava and Klassen (2016) explained this geodesic. However, their definition of the distance between rotations differs from ours based on Eq. (18).

From the definition of the geodesic, Srivastava and Klassen (2016) developed a method of spherical linear interpolation (SLERP) for 3D rotations. We present a brief review of their conclusions considered as an example of the geodesic application.

The geodesic between  $R_{\mathbf{q}_1}$  and  $R_{\mathbf{q}_2}$  can be described by

$$f_l(R_{\mathbf{q}_1}, R_{\mathbf{q}_2}, t) \quad (22)$$

with the affine parameter  $t \in [0, 1]$ . By abuse of notations, in the following context, we denote  $f_l(R_{\mathbf{q}_1}, R_{\mathbf{q}_2}, t)$  by  $f_l(\mathbf{q}_1, \mathbf{q}_2, t)$ . The value of this function is also a unit quaternion representing the rotation. This function describes the relation distance from  $R_{\mathbf{q}_1}$ , i.e.,

$$t = \frac{d_{SO(3)}(\mathbf{q}_1, f_l(\mathbf{q}_1, \mathbf{q}_2, t))}{d_{SO(3)}(\mathbf{q}_1, \mathbf{q}_2)}. \quad (23)$$

Therefore,

$$\begin{aligned} f_l(\mathbf{q}_1, \mathbf{q}_2, 0) &= \mathbf{q}_1, \\ f_l(\mathbf{q}_1, \mathbf{q}_2, 1) &= \mathbf{q}_2. \end{aligned} \quad (24)$$

From the geometry of the geodesic, the analytical formula of the geodesic function can be derived as

$$f_l(\mathbf{q}_1, \mathbf{q}_2, t) = \frac{1}{\sin\phi} (\sin(\phi(1-t))\mathbf{q}_1 + \sin(\phi t)\mathbf{q}_2) \quad (25)$$

if  $\mathbf{q}_1 \cdot \mathbf{q}_2 \geq 0$ , and

$$f_l(\mathbf{q}_1, \mathbf{q}_2, t) = \frac{1}{\sin(\pi - \phi)} (\sin((\pi - \phi)(1-t))\mathbf{q}_1 + \sin((\pi - \phi)t)\mathbf{q}_2) \quad (26)$$

if  $\mathbf{q}_1 \cdot \mathbf{q}_2 < 0$ , where  $\phi = \cos^{-1}(\mathbf{q}_1 \cdot \mathbf{q}_2)$ , ranges  $[0, \pi]$ .

The formula can be used to calculate interpolations between two rotations. As an example, we calculated the interpolation between two rotations  $R_{\mathbf{q}_1} = (-0.884, -0.265, -0.123, 0.364)^T$  and  $R_{\mathbf{q}_2} = (0.370, 0.424, -0.686, -0.461)^T$  (Fig. 2a), and converted the interpolated rotations to Euler angles with the ZYZ convention used in cryoEM (Fig. 2b). From the plots, the changes in the three Euler angles  $\phi$ ,  $\theta$ , and  $\psi$ , are not linear, compared to the linear property of the distance from  $R_{\mathbf{q}_1}$  to the interpolated rotation. Conversely, the linear interpolation of Euler angles does not yield “linear” changes in the rotations. In fact, it is significantly difficult to define a geodesic in the Euler angle system.

### 4. Uniform and quasi-uniform sampling in $SO(3)$

Uniform and quasi-uniform sampling in entire rotational space is frequently used in cryoEM alignment to search for the global optimal solutions of molecular orientations (Grant et al., 2018; Guang Tang et al., 2007; Joachim et al., 1981; Grigorieff, 2018; Plaisier et al., 2007; Punjani et al., 2017; Scheres, 2012; Shaikh Tanvir et al., 2008; Wasilewski and Rosenthal, 2014; Gydo and Alexandre, 2015; Pandurangan et al., 2015). In corresponding methods, the Euler angles and the unit quaternion were used.

The methods used in uniform and quasi-uniform sampling are in two categories. In the first category, sampling points are drawn independently from a uniform distribution (Pandurangan et al., 2015; Liu et al., 2007; Mingxu et al., 2018). The unit quaternion offers a simple approach to generate uniformly distributed unit quaternions  $\{\mathbf{q}_i\}_{1 \leq i \leq N}$  on  $S^3$ , representing uniform distributed rotations  $\{R_{\mathbf{q}_i}\}_{1 \leq i \leq N}$  in  $SO(3)$  (Hamilton, 1844; Kuffner, 2004; Liu et al., 2007; Mardia, 2000). In the second category, based on a quasi-regular grid generated in the rotational space, sampling is performed by sampling at grid points. Such quasi-regular grid sampling can be achieved either by Euler angles in most cryoEM programs (Grant et al., 2018; Guang Tang et al., 2007;

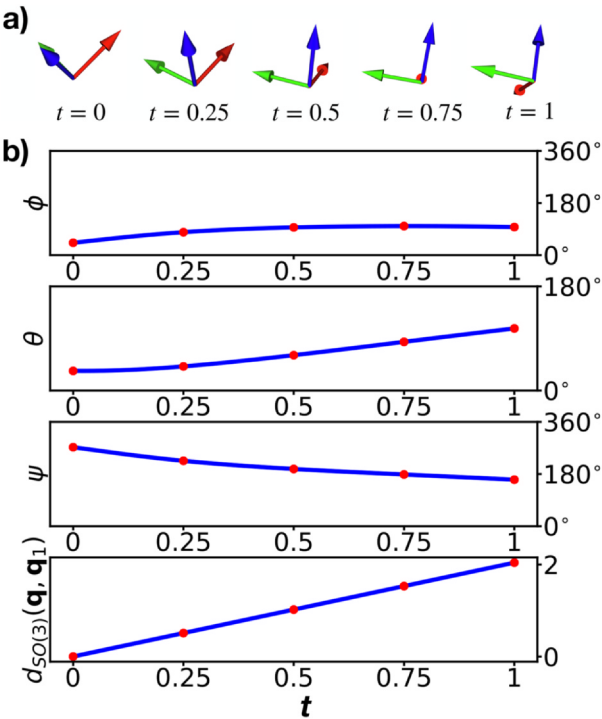


**Fig. 2. Geodesic between two rotations.** Geodesic between two rotations,  $\mathbf{q}_1 = (-0.884, -0.265, -0.123, 0.364)^T$  and  $\mathbf{q}_2 = (0.370, 0.424, -0.686, -0.461)^T$ . **a**, Snapshots of x-axis, y-axis, and z-axis rotated by rotations along the geodesic, where the red arrow indicates the x-axis, the green arrow indicates the y-axis, and the blue arrow indicates the z-axis. **b**, Plots of Z, Y and Z Euler angles and the distance rotating to  $\mathbf{q}_1$  along the geodesic against the affine parameter  $t$ . Red dots correspond to the five snapshots in **a**, respectively.

Joachim et al., 1981; Grigorieff, 2018; Punjani et al., 2017; Scheres, 2012; Shaikh Tanvir et al., 2008), or by unit quaternion (Plaisier et al., 2007; Gydo and Alexandre, 2015). This has shown acceptable coverage of rotational space. A drawback is that sampling points are not independent.

In the first category, i.e., sampling with uniform distribution, two methods have been predominantly used. The first method draws random number  $s$  from uniform distribution ranges  $[0, 1]$  and random numbers  $\theta_1, \theta_2$  from uniform distribution ranges  $[0, 2\pi]$ ; thereafter, the following formula generates unit quaternions uniformly distributed in  $S^3$  (Hamilton, 1844; Kuffner, 2004), i.e.,

$$\begin{aligned} s &\sim U[0, 1] \\ \theta_1 &\sim U[0, 2\pi] \Rightarrow \mathbf{q} = \begin{pmatrix} \sqrt{s} \cos \theta_2 \\ \sqrt{1-s} \sin \theta_1 \\ \sqrt{1-s} \cos \theta_1 \\ \sqrt{s} \sin \theta_2 \end{pmatrix} \sim U_{S^3} \end{aligned} \quad (27)$$

where  $U_{S^3}$  denotes the uniform distribution in  $S^3$ . The second method, uses a 4D Gaussian distribution  $N_4(\mathbf{0}, \mathbf{I})$  with a mean of zero and covariance matrix of a  $4 \times 4$  identity matrix  $\mathbf{I}$  to sample a series of 4D vectors. Thereafter, by normalizing these vectors to have norm 1, we obtain the unit quaternions represented by  $\mathbf{q}$  uniformly distributed in  $S^3$  (Mardia, 2000), i.e.,

$$\mathbf{v} \sim N_4(\mathbf{0}, \mathbf{I}) \Rightarrow \mathbf{q} = \frac{\mathbf{v}}{|\mathbf{v}|} \sim U_{S^3} \quad (28)$$

where  $\mathbf{v}$  is a 4D vector sampled from  $N_4(\mathbf{0}, \mathbf{I})$ , and  $U_{S^3}$  denotes the uniform distribution in  $S^3$ . In both methods, the corresponding rotation  $R_q$  follows a uniform distribution in  $SO(3)$ .

To test the two methods, and adapt the sampling in global search of cryoEM 3D alignment, we generated a set of rotations with uniform distribution using the two methods, and applied on a 2D cryoEM image initially in XY-plane with the normal vector along Z-axis. The resulting

projection directions and in-plane rotational angles by swing-twist decomposition show a uniform distribution (Fig. 3a and b). Liu et al. (2007) applied further selection from uniformly distributed rotations to obtain rotations in a restricted angle range. In  $\mathbf{q} = \left( \hat{\mathbf{n}}_q \sin \frac{\phi}{2} \right)$ ,  $q_0$  relates to rotation angle  $\phi$ , as  $q_0 = \cos \frac{\phi}{2}$ . A uniform sampling was first generated, corresponding to a sampling range in  $[-\phi_0, \phi_0]$ . Thereafter, selecting unit quaternions with  $|\cos \frac{\phi}{2}| \geq \cos \frac{\phi_0}{2}$  results in projection directions that follow uniform distributions in given angle range about the projection axis, and in-plane rotational angles concentrate around  $0^\circ$  (Fig. 3c).

For sampling by quasi-regular grid, two approaches were used. The first (Plaisier et al., 2007; Gydo and Alexandre, 2015) is based on 4D platonic solid (Coxeter, 1973). Apexes of a 4D platonic solid form a quasi-regular grid on  $S^3$ , and are used to generate sampling grid. By selecting the 4D platonic solids with different number of apexes, quasi-regular grids can be obtained with different fineness, summarized and pre-calculated by Karney (2007). We performed a test to generate samplings, and observed the distribution of projection directions and in-plane rotational angles show some regular pattern; hence, quasi-uniform in some extent (Fig. 3d). The second approach involves three steps. Initially, quasi-regular grid is generated on  $S^2$ , presenting the space of projection directions, by either scaled Euler angle method (see Appendix F and Fig. 3e) or HEALPix (Gurski et al., 2005) method (see Fig. 3f). Thereafter, sampling with equal spacing on a unit circle, representing the space of in-plane rotations, is performed. Finally, Cartesian products between projection samplings and in-plane rotation samplings are calculated to obtain a set of quasi-regular grid sampling on  $SO(3)$ . This approach uses Euler angles to represent rotations, and is widely adopted in several cryoEM software (Grant et al., 2018; Guang Tang et al., 2007; Joachim et al., 1981; Grigorieff, 2018; Punjani et al., 2017; Scheres, 2012; Shaikh Tanvir et al., 2008).

In comparison of the sampling methods above, the unit quaternion based methods in the first category shows significant advantages in generating uniform samplings, because they are computationally simple and the sampling points are independent of each other.

## 5. Statistics of rotations in cryoEM

Sampling and randomization in the rotational space is crucial for 3D reconstruction to prevent the so-called local optimization problem or to statistically cover a large rotational space using a limited number of samples. In general, there are two types of requests for random sampling. One is to generate samples in rotational space with a specific statistical distribution. Another one is to estimate the statistical properties for a series of given rotation parameters. Corresponding methods and theories are usually referred to as directional statistics, and the unit quaternion has shown advantages for such purposes. From the distance and geodesic defined above, statistical methods based on the unit quaternion is introduced in the following. First, a method to calculate the average of rotations is reviewed. Second, an angular central Gaussian (ACG) distribution is introduced. Finally, a specific ACG distribution is used as an example to demonstrate a customized application of ACG distribution. From the ACG distribution, we derived a computable formula that is useful in the estimation of the angular precision and angular stability of particles in 3D alignment.

### 5.1. Average rotations

The average of a set of rotations is a simple statistical problem. It is important in statistical analysis for a given distribution, and widely used in cryoEM approaches (Farrow and Ottensmeyer, 1992; Farrow and Ottensmeyer, 1993; Schatz et al., 1997; Georgy and Lamoureux, 2018). From the definition of distance in Eq. (18), the geometric mean (Moakher, 2002) is defined as the average of a given set of rotations

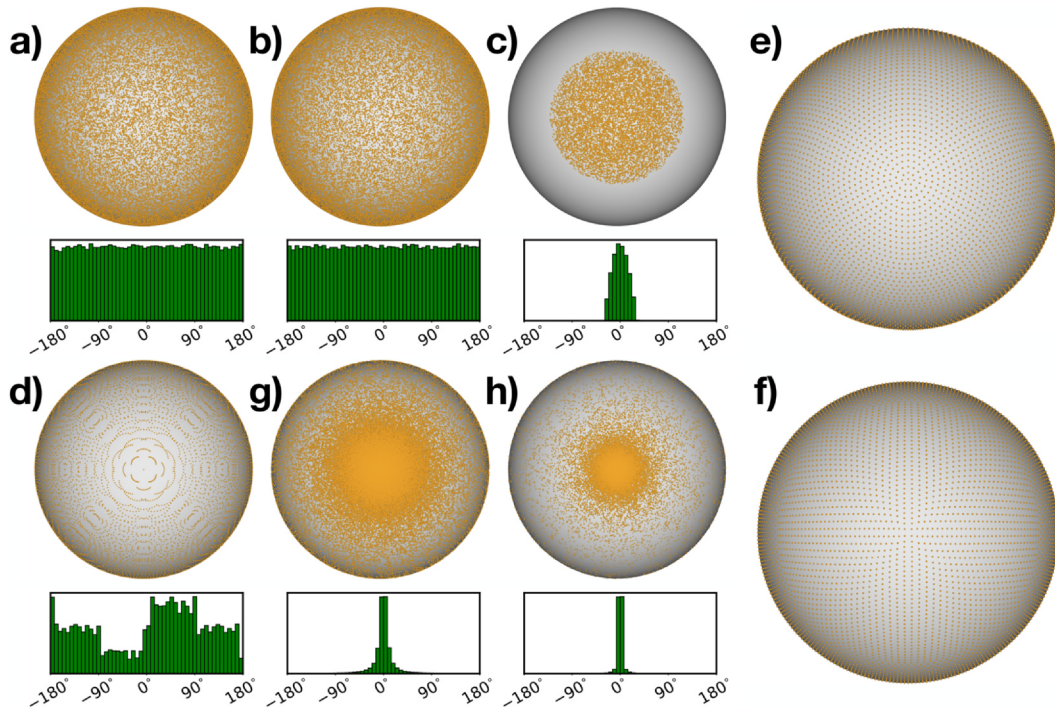


**Fig. 3. Sampling with uniform distribution, Quasi-regular grid, and ACG distribution.** **a**, Plots of the projection directions and in-plane rotation angles of 100,000 rotations sampled with a uniform distribution by Eq. (27). The swing-twist decomposition was used to derive the projection directions and in-plane rotation angles. The scatter plot is for the projection directions, and the bar plot is for the in-plane rotation angles, which are the same for all panels in this figure. **b**, Plots of the projection directions and in-plane rotation angles of 100,000 rotations sampled with a uniform distribution by Eq. (28). **c**, Plots of the projections and in-plane rotations of 10,000 rotations sampled with a uniform distribution by Eq. (27) in a restricted angle of 60°. **d**, Plots of the projections and in-plane rotation angles of the 70,728 grid points from a regular grid, i.e., body-centered cubic lattice c48u2947 in a 48-cell (Karney, 2007), by 4D platonic solid method. **e**, Plot of the regular grid of projection directions at approximate 1.8° interval by scaled Euler method. **f**, Plot of the regular grid of projection directions at approximate 1.8° interval by HEALPix method. **g** and **h** are plots of the projections and in-plane rotation angles of 100,000 rotations sampled with ACG distributions with covariance matrices  $\mathbf{A} = \text{diag}(20^2, 1, 1, 1)$  and  $\mathbf{A} = \text{diag}(100^2, 1, 1, 1)$ , respectively.

$\{R_{\mathbf{q}_i}\}_{1 \leq i \leq N}$  with corresponding weights  $\{w_i\}_{1 \leq i \leq N}$  for each rotation,

$$\arg \min_{R_{\mathbf{q}} \in SO(3)} \sum_{i=1}^N w_i d_{SO(3)}^2(\mathbf{q}, \mathbf{q}_i). \quad (29)$$

However, it is difficult to calculate Eq. (29) (Moakher, 2002). To address this, it was proven that the geometric mean in Eq. (29) can be approximated by the projective arithmetic mean (Oshman and Carmi, 2006) (see Appendix G). Solving the projective arithmetic mean of rotations is a special absolute orientation problem (Slama, 1980) that contributes to the development of the quaternion-assisted angular reconstitution approach (Farrow and Ottensmeyer, 1992; Farrow and Ottensmeyer, 1993) in cryoEM. A solution based on unit quaternion was introduced by Berthold (1987) and Oshman (2007), known as the normalized principal eigenvector of the matrix

$$\mathbf{T} = \sum_{i=1}^N w_i \mathbf{q}_i \mathbf{q}_i^T, \quad (30)$$

where  $\mathbf{q}_i \mathbf{q}_i^T$  is a tensor of  $\mathbf{q}_i$  and itself. Eigenvalues and eigenvectors can be determined using linear algebra techniques. As only the principal eigenvector is required, we use an iterative formula (Jacques, 1987)

$$\bar{\mathbf{q}} \leftarrow \frac{\mathbf{T} \bar{\mathbf{q}}}{|\mathbf{T} \bar{\mathbf{q}}|} \quad (31)$$

to approximate the principal eigenvector. Eq. (31) does not converge only if the largest two eigenvalues of  $\mathbf{T}$  are strictly equal. This nearly never occurs in numerical calculations.

## 5.2. Statistics obtained using ACG distribution

In local search of cryoEM 3D alignment, we often expect to perform

intensive searches around a given rotation (orientation) with high probability. If the distance from the given rotation increases, the probability of determining the accurate solution is decreased; hence, fewer searches are required. Herein, sampling with a Gaussian distribution is used. However, the rotational space is not a linear space, and the Gaussian distribution with a requirement of linear space is not satisfied. Alternatively, the ACG distribution (Tyler, 1987) provides a solution in rotational space with features similar to that of a Gaussian distribution. In general, the ACG distribution is a useful tool in rotational space to generate or analyze samples with a maximal central distribution. THUNDER (Mingxu et al., 2018) used tools of ACG distribution to perform sampling in rotational space.

### 5.2.1. Definition of ACG distribution

Similar to the uniform distribution, the generation and normalization of 4D vectors from Gaussian distribution  $N_4(\mathbf{0}, \mathbf{A})$  with zero mean and covariance matrix  $\mathbf{A}$  leads to unit quaternions that are represented by  $\mathbf{q}$ , follows the ACG distribution (Tyler, 1987)

$$\mathbf{x} \sim N_4(\mathbf{0}, \mathbf{A}) \Rightarrow \mathbf{q} = \frac{\mathbf{v}}{|\mathbf{v}|} \sim \text{ACG}(\mathbf{A}) \quad (32)$$

where  $\mathbf{v}$  is a 4D vector sampled from  $N_4(\mathbf{0}, \mathbf{A})$ , and although  $\mathbf{A}$  is positive definite and symmetric, it is not an identity, that is, different from the identity matrix used in the uniform distribution. The probability density function of the ACG distribution is (Tyler, 1987)

$$p(\mathbf{q}; \mathbf{A}) = |\mathbf{A}|^{-\frac{1}{2}} (\mathbf{q}^T \mathbf{A}^{-1} \mathbf{q})^{-2} \quad (33)$$

and reaches maximum if  $\mathbf{q}$  equals the principal eigenvector of the covariance matrix  $\mathbf{A}$  (Tyler, 1987). Therefore, by selecting a covariance matrix  $\mathbf{A}$  with a principal eigenvector along  $\mathbf{q}$ , we can obtain an ACG

distribution with maximum probability density at  $\mathbf{q}$ . As an example, Fig. 3g and h demonstrate the distribution of projection directions and in-plane rotational angles of samplings with ACG distribution, where  $\mathbf{A}$  are diagonal matrices with principal eigenvector along  $(1, 0, 0, 0)^T$ . A method is introduced to generate such a covariance matrix (see Appendix H).

Given a set of unit quaternions  $\{\mathbf{q}_i\}_{1 \leq i \leq N}$ , the estimation for covariance matrix  $\mathbf{A}$  is useful in probability analysis and generating new random rotations. Whereas missing an explicit maximum-likelihood method to estimate  $\mathbf{A}$ , an iterative formula (Tyler, 1987) is usually used to approximate  $\mathbf{A}$

$$\mathbf{A}^{(k+1)} = 4 \left\{ \sum_{i=1}^N \frac{1}{\mathbf{q}_i^T \mathbf{A}^{(k)} \mathbf{q}_i} \right\}^{-1} \left\{ \sum_{i=1}^N \frac{\mathbf{q}_i \mathbf{q}_i^T}{\mathbf{q}_i^T \mathbf{A}^{(k)} \mathbf{q}_i} \right\}. \quad (34)$$

### 5.2.2. Local perturbation and confidence area

As mentioned before, a set of rotations  $\{R_{\mathbf{q}_i}\}_{1 \leq i \leq N}$  can be generated using an ACG distribution around a given rotation  $R_{\bar{\mathbf{q}}}$  by selecting a covariance matrix  $\mathbf{A}$ . Herein, we use a special form of covariance matrix to generate rotations that can be conveniently correlated with the angular accuracy of local search in cryoEM.

To obtain  $\{R_{\mathbf{q}_i}\}_{1 \leq i \leq N}$ , we first generate a set of unit quaternions  $\{\mathbf{q}_i\}_{1 \leq i \leq N}$  with an ACG distribution  $ACG(A)$ , wherein a special covariance matrix

$$\mathbf{A} = \begin{pmatrix} k^2 & & & \\ & 1 & & \\ & & 1 & \\ & & & 1 \end{pmatrix} \quad (35)$$

is selected with  $k > 1$  so that the principal eigenvector of  $\mathbf{A}$  is along  $\mathbf{q}_e = (1, 0, 0, 0)^T$ ,  $R_{\mathbf{q}_e}$  is a still rotation, i.e., no rotation. Accordingly,  $\{R_{\mathbf{q}_i}\}_{1 \leq i \leq N}$  present perturbations for the still rotation. By appending these generated rotations to a given rotation  $R_{\bar{\mathbf{q}}}$ , i.e.,  $\bar{\mathbf{q}} \otimes \mathbf{q}'_i$ , we obtain perturbations  $\{R_{\mathbf{q}_i}\}_{1 \leq i \leq N}$  for  $R_{\bar{\mathbf{q}}}$  as

$$\{R_{\mathbf{q}_i}\}_{1 \leq i \leq N} = \{R_{\bar{\mathbf{q}} \otimes \mathbf{q}'_i}\}_{1 \leq i \leq N} \quad (36)$$

which still follows a specific ACG distribution.

In the covariance matrix  $\mathbf{A}$ , the parameter  $k$  is used to regulate the range of perturbations. A larger  $k$  value leads to a narrower distribution of  $\{\mathbf{q}_i\}_{1 \leq i \leq N}$  in  $S^3$ , i.e., perturbations over a smaller range. For the local search in cryoEM 3D alignment, the range of perturbations is directly correlated to the angular accuracy of orientation search. In the following, we develop the relationship between  $k$  and the angular accuracy of the local search, which may be used to generate a perturbation with a given accuracy requirement.

Considering an arbitrary unit vector  $\vec{v}_0$  and a resulting unit vector  $\vec{v}$  from rotating  $\vec{v}_0$  by  $\mathbf{q} \sim ACG(\mathbf{A})$  with  $\mathbf{A}$  in Eq. (35), the inner product of  $\vec{v}$  and  $\vec{v}_0$ ,  $z = \vec{v} \cdot \vec{v}_0 \in [-1, 1]$ , equals the cosine of their angular distance. The angular distance, i.e.,  $\cos^{-1}(z)$ , reflects the intensity of the perturbation obtained by  $\mathbf{q}$ .

To characterize the intensity of the perturbation, we first derived the probability density of the resulting unit vector  $\vec{v}$ , which is (see Appendix I)

$$p(\vec{v}; \vec{v}_0, \mathbf{A}) = \frac{1}{2\sqrt{2}k} \frac{\left(\frac{1}{k^2} - 1\right)z + \left(\frac{1}{k^2} + 3\right)}{\left(\left(\frac{1}{k^2} - 1\right)z + \left(\frac{1}{k^2} + 1\right)\right)^{\frac{3}{2}}} \quad (37)$$

where  $p(\vec{v}; \vec{v}_0, \mathbf{A})$  reaches maximum if  $z = \vec{v} \cdot \vec{v}_0 = 1$ , i.e.,  $\vec{v} = \vec{v}_0$ , and  $\vec{v}$  follows a distribution invariant under rotation around  $\vec{v}_0$  (Appendix I, Fig. 4a). Thereafter, we introduce the concept of confidence area  $[z_0, 1]$  under a confidence level  $a$  that satisfies

$$\int_{\{\vec{v} | \vec{v} \cdot \vec{v}_0 \in [z_0, 1]\}} p(\vec{v}; \vec{v}_0, \mathbf{A}) d\vec{v} = a. \quad (38)$$

The confidence level  $a$  describes the probability of making a perturbation up to  $z_0$ , or up to the angle distance of  $\cos^{-1}(z_0)$  (Fig. 4b). That

is, the confidence level can also be considered as the percentage of samples fallen in a range with angle distance up to  $\cos^{-1}(z_0)$ . Therefore,  $\epsilon = \cos^{-1}(z_0)$ , can be defined as the angular precision of rotation sampling under a given confidence level,  $a$ . We developed the following formula to calculate  $z_0$  with given  $k$  and  $a$  (see Appendix J)

$$\begin{aligned} z_0 &= \frac{z_0^2 - \left(\frac{1}{k^2} + 1\right)}{\frac{1}{k^2} - 1}, \\ z_0' &= \frac{a' + \sqrt{a'^2 + 8}}{2}, \\ a' &= \frac{\sqrt{2}(1-k^2)(1-a)}{k}. \end{aligned} \quad (39)$$

To simplify the computation, we derive an approximation formula to calculate angular precision  $\epsilon$  from  $k$  and  $a$ , or to calculate  $k$  from  $\epsilon$  and  $a$ , as

$$\frac{1}{\epsilon} = \frac{1-a}{2\sqrt{2a-a^2}}k \quad (40)$$

In particular, this formula is the asymptote of  $\frac{1}{\epsilon}$  if  $k \rightarrow \infty$  (Fig. 4b). The correctness of this approximation formula is proven in Appendix K.

### 5.2.3. Inference based on ACG distribution

In the particle-filter algorithm implemented in THUNDER (Mingxu et al., 2018), the posterior probability density function of the rotation estimates is described by the distribution of a series of rotations  $\{R_{\mathbf{q}_i}\}_{1 \leq i \leq N}$ . This generates the requirement for the inference of distribution of  $\{R_{\mathbf{q}_i}\}_{1 \leq i \leq N}$ .

Considering the inverse process of the previous section,  $\{R_{\mathbf{q}_i}\}_{1 \leq i \leq N}$  can be considered as perturbations for their average  $\bar{\mathbf{q}}$ . Thus,  $\bar{\mathbf{q}}^{-1} \otimes \mathbf{q}_i$  or corresponding rotations  $\{R_{\bar{\mathbf{q}}^{-1} \otimes \mathbf{q}_i}\}_{1 \leq i \leq N}$  are the perturbations for still rotation  $\mathbf{q}_e = (1, 0, 0, 0)^T$ . For simplicity, we assume that  $\{R_{\bar{\mathbf{q}}^{-1} \otimes \mathbf{q}_i}\}_{1 \leq i \leq N}$ , follows the ACG distribution, and has a covariance matrix in Eq. (35). Thereafter, we develop an iterative method to determine the maximum-likelihood approximation of  $k$  from  $\{\bar{\mathbf{q}}^{-1} \otimes \mathbf{q}_i\}_{1 \leq i \leq N}$ , which is

$$k^2 = \frac{4}{N} \sum_{i=1}^N \frac{q_{0i}^2}{k^{-2}q_{0i}^2 + \vec{n}_{\mathbf{q}_i} \cdot \vec{n}_{\mathbf{q}_i}} \quad (41)$$

where  $\begin{pmatrix} q_{0i} \\ \vec{n}_{\mathbf{q}_i} \end{pmatrix} = \bar{\mathbf{q}}^{-1} \otimes \mathbf{q}_i$ . The correctness of this iterative method is proven in Appendix L.

Combining Eq. (39) with Eq. (41), we developed a method to estimate the angular precision of the parameter search from a series of samples generated by the particle-filter algorithm in THUNDER (Mingxu et al., 2018). As an example, we performed the ab initio 3D reconstruction of a dataset of the proteasome (EMPIAR-10025) using 112,412 particles. A global search was performed under three sequentially increasing cutoff frequencies, 56.1 Å, 16.8 Å, and 9.9 Å. For each cutoff frequency, the average angular precision of all particles increased and converged (Fig. 5, blue, red, and orange dots, respectively). During a local search, as the cutoff frequency increased in each round from 9.9 Å to 2.69 Å, the average angular precision rapidly increased from 1.42° and then converged at 0.704° (Fig. 5, violet dots). Finally, defocus refinement was performed. As the resolution increased from 2.47 Å to 2.33 Å, the angular precision was improved to 0.661° (Fig. 5, blue dots).

## 6. Molecular symmetry by unit quaternion

In cryoEM 3D reconstruction and alignment, molecular symmetry is an important property that can be used to enhance the signal and reduce the computation. In this section, we show how to apply unit quaternions to simplify calculations in the presence of molecular symmetry.

As molecules are chiral in cryoEM, there are only five classes of molecular symmetry groups. These are the cyclic group ( $C_n$ ), dihedral group ( $D_n$ ), tetrahedral group ( $T$ ), octahedral group ( $O$ ), and

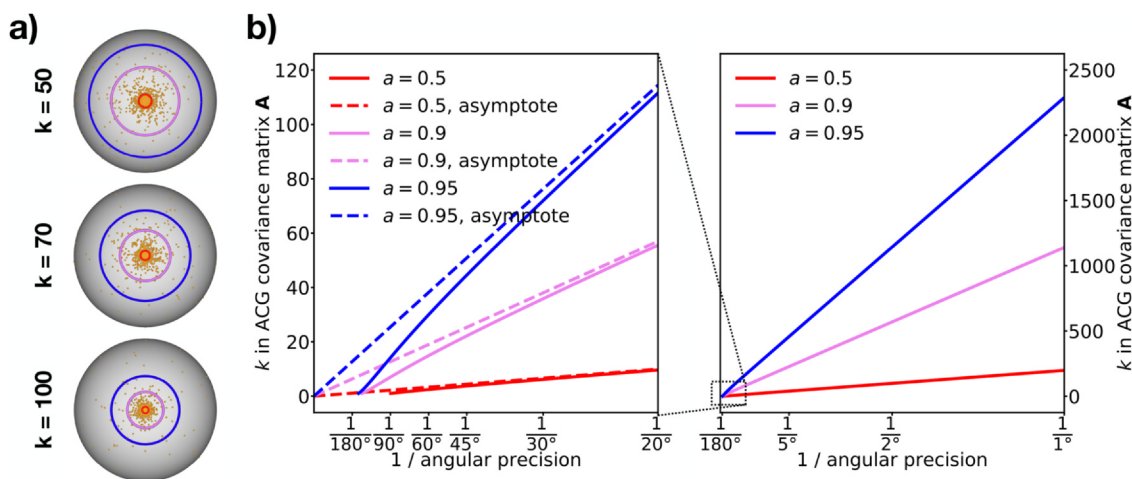


**Fig. 4. ACG distribution with different covariance matrix parameter  $k$ .** **a**, distributions with  $k$  equals to 50, 70, and 100. In each plot, 3000 rotations are sampled from an ACG distribution with a covariance matrix of  $\text{diag}(k^2, 1, 1)$ . The resulting vectors rotated from  $(0, 0, 1)^T$  are plotted as orange points. Boundaries of the confidence area with multiple confidence level  $a$  of 0.5, 0.9, and 0.95 are shown as red, violet, and blue circles, respectively. **b**, The correlation between  $k$  in the ACG covariance matrix  $\mathbf{A}$  and the reciprocal of the angular precision. Multiple confidence levels are plotted. Dashed lines indicate the asymptotes of this correlation.

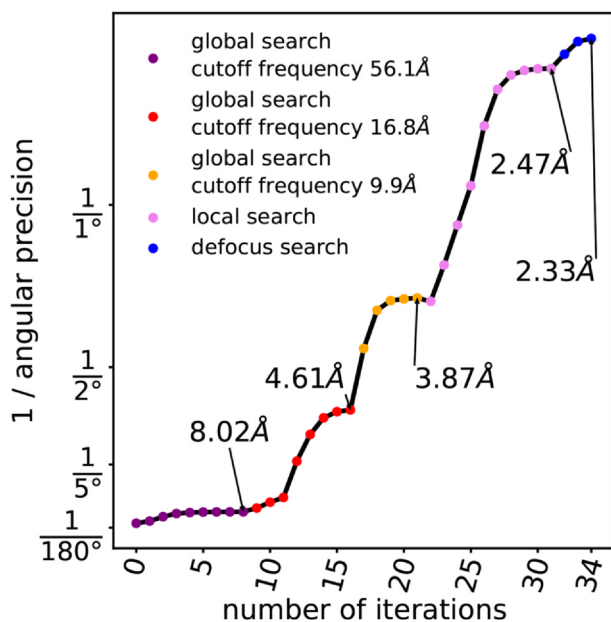


**Fig. 5. The angular precision increases as the refinement is iterated.** 3D refinement is performed using a proteasome dataset (EMPIAR-10025) with 112,412 particles and an ellipsoid as initial model. The reciprocal of the average angular precision is plotted against the iteration number of refinement. A global search is performed under three sequentially increasing cutoff frequencies, followed by a local search and a defocus search. The resolutions of the refining reference at several iterative rounds are labeled.

icosahedral group ( $I$ ). Using unit quaternions, the symmetric operations of these symmetry groups can be calculated conveniently, from no more than two generators introduced by Conway and Smith (2003). Based on Conway's method, we derived the generators of these molecular symmetry groups under the orientation conventions in cryoEM (Table 1). The cyclic group is the simplest one, and has only one generator. The other four groups need two generators.

In 3D alignment, the sampling should be performed in the entire rotational space. If molecular symmetry exists, only the sampling in an asymmetric unit is required. However, the asymmetric unit varies under different definitions. We usually initially fix a central rotation  $R_{\mathbf{q}_0}$ , and then define the asymmetric unit  $D(R_{\mathbf{q}_0})$  under symmetry group  $G$  as

$$D(R_{\mathbf{q}_0}) := \{R_{\mathbf{q}} \mid d_{SO(3)}(\mathbf{q}, \mathbf{q}_0) \leq d_{SO(3)}(\mathbf{q} \otimes \mathbf{q}_g, \mathbf{q}_0), \forall \mathbf{q}_g \in G\} \quad (42)$$

where  $\mathbf{q}_g$  is a symmetric operation in  $G$ , and  $\mathbf{q} \otimes \mathbf{q}_g$  is a symmetrically related unit quaternion of  $\mathbf{q}$ . To achieve sampling in the asymmetry unit  $D(R_{\mathbf{q}_0})$ , we calculate all possible values of  $\mathbf{q} \otimes \mathbf{q}_g$ , and select one closest to  $\mathbf{q}_0$ .

An asymmetric unit is convex. This implies that the geodesic between any two rotations in an asymmetric unit lies inside the asymmetric unit. This property ensures that the SLERP interpolation between any two rotations in an asymmetric unit is in the same asymmetric unit.

## 7. Discussion

Rotational operations and analyses are extensively used in cryoEM image analysis and 3D reconstruction. Unit quaternion systems have been shown as convenient and mathematically rigorous tools to manage and analyze the orientations of molecules or their projections, and can be competitive alternative for the Euler angle system. A disadvantage of the unit quaternion is, it is not intuitive compared to the Euler angles in representing the in-plane rotation and 3D orientation change. The swing-twist decomposition addresses this problem.

In particular, the rotation operations represented by unit quaternions are significantly correlated with the 4D vector in the  $S^3$  sphere in 4D space. Accordingly, the properties of rotation can be directly derived and converted to the analysis of the 4D unit vectors. This leads to the definition of the distance and geodesic. The former enables direct comparison of rotations, and is useful in the diagnosis of orientation stability of particles in 3D alignment. The latter enables interpolation and analysis for continuous changes of rotations that can be used in the analysis of flexible samples. With distance and geodesic being well defined, statistics tools are established for 3D cryoEM image processing. Two types of distributions, uniform and ACG, were developed from the 4D Gaussian distribution of 4D vectors. These distribution models provide powerful tools of sampling and inference of either global or local optimization of molecule orientations.

In summary, unit quaternions can perform significant roles in the future cryoEM algorithms. Well-defined statistical tools for unit quaternions form comprehensive systems for analyzing spatial rotations, and providing significant freedom if processing and understanding the orientation optimization in cryoEM.

**Table 1**  
Molecular symmetry groups.

Symmetry Group	Symbol	Generators	Axis of Generators	Number of Elements
Cyclic	$C_n$	$\left(\cos\frac{\pi}{n}, 0, 0, \sin\frac{\pi}{n}\right)^T$	$C_n$ on $Z$	$n$
Dihedral	$D_n$	$\left(\cos\frac{\pi}{n}, 0, 0, \sin\frac{\pi}{n}\right)^T, (0, 1, 0, 0)^T$	$C_n$ on $Z, C_2$ on $X$	$2n$
Tetrahedral	$T$	$\left(\frac{1}{2}, 0, 0, \frac{\sqrt{3}}{2}\right)^T, \left(0, 0, \frac{\sqrt{6}}{3}, \frac{\sqrt{3}}{3}\right)^T$	$C_3$ on $Z, C_2$ on $\left(0, \frac{\sqrt{6}}{3}, \frac{\sqrt{3}}{3}\right)^T$	12
Octahedral	$O$	$\left(\frac{\sqrt{2}}{2}, 0, 0, \frac{\sqrt{2}}{2}\right)^T, \left(\frac{1}{2}, \frac{1}{2}, \frac{1}{2}, \frac{1}{2}\right)^T$	$C_4$ on $Z, C_3$ on $\left(\frac{1}{\sqrt{3}}, \frac{1}{\sqrt{3}}, \frac{1}{\sqrt{3}}\right)^T$	24
Icosahedral	$I$	$(0, 0, 0, 1)^T, \left(\frac{1}{2}, 0, \frac{\sqrt{5}-1}{4}, \frac{\sqrt{5}+1}{4}\right)^T$	$C_2$ on $Z, C_3$ on $\left(0, \frac{\sqrt{5}-1}{2\sqrt{3}}, \frac{\sqrt{5}+1}{2\sqrt{3}}\right)^T$	60

### Declaration of Competing Interest

The authors declare that they have no known competing financial interests or personal relationships that could have appeared to influence the work reported in this paper.

### Acknowledgements

This work was supported by funds from the National Key Research

### Appendix A. Gimbal lock

There are two types of Euler angles based on the selection of rotation axes. Euler angles with fixed rotation axes are referred as extrinsic Euler angles, and those with rotating rotation axes are referred as intrinsic Euler angles.

Gimbal lock problem occurs in intrinsic Euler angles. Herein, if two rotating rotation axes overlap, a degree of freedom is lost. Consequently, some rotations cannot be represented by Euler angles that rotate about the given rotation axes.

### Appendix B. Basic quaternion algebra property

Herein, we describe some basic properties of quaternion algebra. Readers may refer to [Vince \(2011\)](#) for further details. The following properties of quaternions are similar to complex numbers, except that the multiplication of quaternions is not commutative, i.e.,  $\mathbf{q}_1 \otimes \mathbf{q}_2$  is not always equal to  $\mathbf{q}_2 \otimes \mathbf{q}_1$ .

The inverse of a non-zero quaternion  $\mathbf{q}$ , denoted by  $\mathbf{q}^{-1}$ , is defined as the quaternion that satisfies  $\mathbf{q}^{-1} \otimes \mathbf{q} = 1$  and  $\mathbf{q} \otimes \mathbf{q}^{-1} = 1$ . By quaternion multiplication, i.e., Eq. (6), the product of quaternion  $\mathbf{q}$  and its conjugate  $\mathbf{q}^*$  (Eq. (3)) is given by

$$\begin{aligned} \mathbf{q} \otimes \mathbf{q}^* &= \begin{pmatrix} q_0 \\ \vec{n}_q \end{pmatrix} \otimes \begin{pmatrix} q_0 \\ -\vec{n}_q \end{pmatrix} \\ &= \begin{pmatrix} q_0^2 + \vec{n}_q \cdot \vec{n}_q \\ 0 \end{pmatrix} \\ &= \begin{pmatrix} |\mathbf{q}|^2 \\ 0 \end{pmatrix}, \end{aligned} \quad (43)$$

which is usually written as  $\mathbf{q} \otimes \mathbf{q}^* = |\mathbf{q}|^2$ . Similarly,  $\mathbf{q}^* \otimes \mathbf{q} = |\mathbf{q}|^2$ . Accordingly,  $\mathbf{q}^{-1}$  can be calculated as

$$\mathbf{q}^{-1} = \frac{\mathbf{q}^*}{|\mathbf{q}|^2}. \quad (44)$$

If  $\mathbf{q}$  is a unit quaternion,  $|\mathbf{q}| = 1$  and  $\mathbf{q}^{-1} = \mathbf{q}^*$ .

The conjugation, norm, and multiplication of quaternions satisfies the following properties.

- (i)  $(\mathbf{q}^*)^* = \mathbf{q}$ .
- (ii)  $(\mathbf{q}_1 \otimes \mathbf{q}_2)^* = \mathbf{q}_2^* \otimes \mathbf{q}_1^*$ .
- (iii)  $|\mathbf{q}| = |\mathbf{q}^*|$ .
- (iv)  $|\mathbf{q}_1 \otimes \mathbf{q}_2| = |\mathbf{q}_1| \cdot |\mathbf{q}_2|$ .
- (v) Multiplication is associative, i.e.,  $(\mathbf{q}_1 \otimes \mathbf{q}_2) \otimes \mathbf{q}_3 = \mathbf{q}_1 \otimes (\mathbf{q}_2 \otimes \mathbf{q}_3)$ .
- (vi) 1 is the multiplicative identity, i.e.,  $1 \otimes \mathbf{q} = \mathbf{q} \otimes 1 = \mathbf{q}$ .

Denoting the set of all unit quaternions  $\{\mathbf{q} | |\mathbf{q}| = 1\}$  by  $S^3$  that is a 3-dimensional sphere in  $\mathbb{R}^4$ ,  $S^3$  is closed under the multiplication of quaternions, hence, it is a group. Moreover,  $S^3$  is a compact and Hausdorff topological subspace of  $\mathbb{R}^4$ , and the multiplication of unit quaternions is continuous. Therefore,  $S^3$  is a compact topological group. In fact,  $S^3$  is a compact Lie group ([Stillwell, 2008](#)).

### Appendix C. Converting Euler angles to unit quaternion

Because the rotation by Euler angles  $\phi$ ,  $\theta$ , and  $\psi$  in ZYZ convention is a combination of rotating  $\phi$  about the  $z$ -axis, followed by rotating  $\theta$  about the  $y$ -axis, and finally rotating  $\psi$  about the  $z$ -axis, the corresponding unit quaternion is

$$\mathbf{q}_{\phi\theta\psi} = \mathbf{q}_\psi \otimes \mathbf{q}_\theta \otimes \mathbf{q}_\phi, \quad (45)$$

where

$$\mathbf{q}_\phi = \begin{pmatrix} \cos \frac{\phi}{2} \\ 0 \\ 0 \\ \sin \frac{\phi}{2} \end{pmatrix}, \mathbf{q}_\theta = \begin{pmatrix} \cos \frac{\theta}{2} \\ 0 \\ \sin \frac{\theta}{2} \\ 0 \end{pmatrix}, \mathbf{q}_\psi = \begin{pmatrix} \cos \frac{\psi}{2} \\ 0 \\ 0 \\ \sin \frac{\psi}{2} \end{pmatrix}. \quad (46)$$

Thus, the corresponding unit quaternion  $\mathbf{q}_{\phi\theta\psi}$  can be calculated as

$$\mathbf{q}_{\phi\theta\psi} = \begin{pmatrix} \cos \frac{\theta}{2} \cos \frac{\psi + \phi}{2} \\ -\sin \frac{\theta}{2} \sin \frac{\psi - \phi}{2} \\ \sin \frac{\theta}{2} \cos \frac{\psi - \phi}{2} \\ \cos \frac{\theta}{2} \sin \frac{\psi + \phi}{2} \end{pmatrix}. \quad (47)$$

### Appendix D. Conversion between unit quaternion and rotation matrix

A  $3 \times 3$  rotation matrix  $\mathbf{M}$  can be converted to the unit quaternion  $\mathbf{q}$  or  $-\mathbf{q}$  by

$$\begin{aligned} f_{\mathbf{M} \rightarrow \mathbf{q}} & \left( \begin{pmatrix} a_{00} & a_{01} & a_{02} \\ a_{10} & a_{11} & a_{12} \\ a_{20} & a_{12} & a_{22} \end{pmatrix} \right) \\ &= \pm \begin{pmatrix} \frac{1}{2} \sqrt{1 + a_{00} + a_{11} + a_{22}} \\ \frac{1}{2} \frac{a_{21} - a_{12}}{|a_{21} - a_{12}|} \sqrt{1 + a_{00} - a_{11} - a_{22}} \\ \frac{1}{2} \frac{a_{02} - a_{20}}{|a_{02} - a_{20}|} \sqrt{1 - a_{00} + a_{11} - a_{22}} \\ \frac{1}{2} \frac{a_{10} - a_{01}}{|a_{10} - a_{01}|} \sqrt{1 - a_{00} - a_{11} + a_{22}} \end{pmatrix}, \end{aligned} \quad (48)$$

A unit quaternion  $\mathbf{q}$  can be converted to a  $3 \times 3$  rotation matrix  $\mathbf{M}$  by

$$f_{\mathbf{q} \rightarrow \mathbf{R}} \left( \begin{pmatrix} q_0 \\ q_1 \\ q_2 \\ q_3 \end{pmatrix} \right) = \mathbf{I} + 2q_0 \mathbf{A} + 2\mathbf{A}\mathbf{A}, \quad (49)$$

where  $\mathbf{I}$  is a  $3 \times 3$  unit matrix, and

$$\mathbf{A} = \begin{pmatrix} 0 & -q_3 & q_2 \\ q_3 & 0 & -q_1 \\ -q_2 & q_1 & 0 \end{pmatrix}. \quad (50)$$

### Appendix E. Distance between rotations

#### E.1. Proof of well-definedness of distance between two rotations

In this section, Eq. (18) will be proven to be a well-defined distance definition in  $SO(3)$ .

First, the maximum definition of distance between two rotations  $R_{\mathbf{q}_1}, R_{\mathbf{q}_2} \in SO(3)$ , i.e., Eq. (18), can be attained as  $S^2$  is compact. Thus, the use of the maximum operator is appropriate in Eq. (18).

Second, it will be proven below that the three basic requirements of the distance definition in mathematics, i.e., the symmetry property, the positive definiteness property, and the triangle inequality property, are satisfied for Eq. (18).

The symmetry property is such that

$$d_{SO(3)}(\mathbf{q}_1, \mathbf{q}_2) = d_{SO(3)}(\mathbf{q}_2, \mathbf{q}_1) \quad (51)$$

holds for all  $\mathbf{q}_1, \mathbf{q}_2 \in SO(3)$ . Our proof is as follows.

$$\begin{aligned}
d_{SO(3)}(\mathbf{q}_1, \mathbf{q}_2) &= \max_{\vec{\mathbf{v}} \in S^2} d_{S^2}(R_{\mathbf{q}_1}(\vec{\mathbf{v}}), R_{\mathbf{q}_2}(\vec{\mathbf{v}})) \\
&= \max_{\vec{\mathbf{v}} \in S^2} d_{S^2}(R_{\mathbf{q}_2}(\vec{\mathbf{v}}), R_{\mathbf{q}_1}(\vec{\mathbf{v}})) \\
&= d_{SO(3)}(\mathbf{q}_2, \mathbf{q}_1)
\end{aligned} \tag{52}$$

as  $d_{S^2}(R_{\mathbf{q}_1}(\vec{\mathbf{v}}), R_{\mathbf{q}_2}(\vec{\mathbf{v}})) = d_{S^2}(R_{\mathbf{q}_2}(\vec{\mathbf{v}}), R_{\mathbf{q}_1}(\vec{\mathbf{v}}))$  holds, because  $d_{S^2}$ , i.e., distance in  $S^2$ , also has symmetry property.

The positive definiteness property contains two parts. The first part is

$$d_{SO(3)}(\mathbf{q}_1, \mathbf{q}_2) \geq 0 \tag{53}$$

holds for all  $R_{\mathbf{q}_1}, R_{\mathbf{q}_2} \in SO(3)$ . This can be derived from  $d_{S^2}(R_{\mathbf{q}_1}(\vec{\mathbf{v}}), R_{\mathbf{q}_2}(\vec{\mathbf{v}})) \geq 0$  for any  $\vec{\mathbf{v}} \in S^2$ , as  $d_{S^2}$  is the distance in  $S^2$  that has a positive definiteness property. The second part is

$$d_{SO(3)}(\mathbf{q}_1, \mathbf{q}_2) = 0 \tag{54}$$

holds if and only if  $R_{\mathbf{q}_1} = R_{\mathbf{q}_2}$ . This statement is proven as follows. If  $R_{\mathbf{q}_1} = R_{\mathbf{q}_2}$ ,  $R_{\mathbf{q}_1}(\vec{\mathbf{v}}) = R_{\mathbf{q}_2}(\vec{\mathbf{v}})$  for any  $\vec{\mathbf{v}} \in S^2$  that yields  $d_{S^2}(R_{\mathbf{q}_1}(\vec{\mathbf{v}}), R_{\mathbf{q}_2}(\vec{\mathbf{v}})) = 0$  for any  $\vec{\mathbf{v}} \in S^2$ , and  $d_{SO(3)}(R_{\mathbf{q}_1}, R_{\mathbf{q}_2}) = 0$ . Conversely, if  $d_{SO(3)}(R_{\mathbf{q}_1}, R_{\mathbf{q}_2}) = 0$ , for any  $\vec{\mathbf{v}} \in S^2$ ,  $d_{S^2}(R_{\mathbf{q}_1}(\vec{\mathbf{v}}), R_{\mathbf{q}_2}(\vec{\mathbf{v}})) = 0$ , i.e.,  $R_{\mathbf{q}_1}(\vec{\mathbf{v}}) = R_{\mathbf{q}_2}(\vec{\mathbf{v}})$ ; that is,  $R_{\mathbf{q}_1} = R_{\mathbf{q}_2}$ .

The triangle inequality property indicates that

$$d_{SO(3)}(\mathbf{q}_1, \mathbf{q}_2) \leq d_{SO(3)}(\mathbf{q}_1, \mathbf{q}_3) + d_{SO(3)}(\mathbf{q}_3, \mathbf{q}_2) \tag{55}$$

holds for all  $R_{\mathbf{q}_1}, R_{\mathbf{q}_2}, R_{\mathbf{q}_3} \in SO(3)$ . Therefore,

$$\begin{aligned}
&d_{SO(3)}(\mathbf{q}_1, \mathbf{q}_2) \\
&= \max_{\vec{\mathbf{v}} \in S^2} d_{S^2}(R_{\mathbf{q}_1}(\vec{\mathbf{v}}), R_{\mathbf{q}_2}(\vec{\mathbf{v}})) \\
&\leq \max_{\vec{\mathbf{v}} \in S^2} (d_{S^2}(R_{\mathbf{q}_1}(\vec{\mathbf{v}}), R_{\mathbf{q}_3}(\vec{\mathbf{v}})) + d_{S^2}(R_{\mathbf{q}_3}(\vec{\mathbf{v}}), R_{\mathbf{q}_2}(\vec{\mathbf{v}}))) \\
&\leq \max_{\vec{\mathbf{v}} \in S^2} d_{S^2}(R_{\mathbf{q}_1}(\vec{\mathbf{v}}), R_{\mathbf{q}_3}(\vec{\mathbf{v}})) + \max_{\vec{\mathbf{v}} \in S^2} d_{S^2}(R_{\mathbf{q}_3}(\vec{\mathbf{v}}), R_{\mathbf{q}_2}(\vec{\mathbf{v}})) \\
&= d_{SO(3)}(\mathbf{q}_1, \mathbf{q}_3) + d_{SO(3)}(\mathbf{q}_3, \mathbf{q}_2)
\end{aligned} \tag{56}$$

as  $d_{S^2}(R_{\mathbf{q}_1}(\vec{\mathbf{v}}), R_{\mathbf{q}_2}(\vec{\mathbf{v}})) \leq d_{S^2}(R_{\mathbf{q}_1}(\vec{\mathbf{v}}), R_{\mathbf{q}_3}(\vec{\mathbf{v}})) + d_{S^2}(R_{\mathbf{q}_3}(\vec{\mathbf{v}}), R_{\mathbf{q}_2}(\vec{\mathbf{v}}))$  holds because  $d_{S^2}$ , i.e., the distance in  $S^2$  also satisfies the triangle inequality property.

We have proven the suitability of Eq. (18) as a distance definition between two rotations.

## E.2. Rotation distance calculated using unit quaternions

In this section, we show that Eq. (20) and Eq. (19) are equivalent to the distance in  $SO(3)$  defined by Eq. (18) using the unit quaternion.

We first prove that Eq. (19) is equals to the distance definition Eq. (18). This proof contains two steps. First, we show that the distance between  $R_{\mathbf{q}_1}$  and  $R_{\mathbf{q}_2}$  in  $SO(3)$  using Eq. (18) equals the angle of rotation of  $R_{\mathbf{q}_1^{-1} \otimes \mathbf{q}_2}$ . Second,  $2\cos^{-1}(|\mathbf{q}_1 \cdot \mathbf{q}_2|)$ , obtained from Eq. (19) will be shown to be equal to the angle of rotation of  $R_{\mathbf{q}_1^{-1} \otimes \mathbf{q}_2}$ .

The first step, i.e.,  $d_{SO(3)}(\mathbf{q}_1, \mathbf{q}_2)$  in Eq. (18) equals the angle of rotation of  $R_{\mathbf{q}_1^{-1} \otimes \mathbf{q}_2}$ , is proven as follows.

$d_{SO(3)}$  has the following properties. The right multiplication of the same rotation  $R_{\mathbf{q}}$  maintains the distance such that

$$d_{SO(3)}(\mathbf{q}_1 \otimes \mathbf{q}, \mathbf{q}_2 \otimes \mathbf{q}) = d_{SO(3)}(\mathbf{q}_1, \mathbf{q}_2) \tag{57}$$

holds for all  $R_{\mathbf{q}_1}, R_{\mathbf{q}_2}$  and  $R_{\mathbf{q}}$ . The left multiplication of the same rotation  $R_{\mathbf{q}}$  also maintains the distance such that

$$d_{SO(3)}(\mathbf{q} \otimes \mathbf{q}_1, \mathbf{q} \otimes \mathbf{q}_2) = d_{SO(3)}(\mathbf{q}_1, \mathbf{q}_2) \tag{58}$$

holds for all  $R_{\mathbf{q}_1}, R_{\mathbf{q}_2}$  and  $R_{\mathbf{q}}$ .

The right multiplication distance-preserving property, i.e., Eq. (57), holds as

$$\begin{aligned}
d_{SO(3)}(\mathbf{q}_1 \otimes \mathbf{q}, \mathbf{q}_2 \otimes \mathbf{q}) &= \max_{\vec{\mathbf{v}} \in S^2} d_{S^2}(R_{\mathbf{q}_1 \otimes \mathbf{q}}(\vec{\mathbf{v}}), R_{\mathbf{q}_2 \otimes \mathbf{q}}(\vec{\mathbf{v}})) \\
&= \max_{\vec{\mathbf{v}} \in S^2} d_{S^2}(R_{\mathbf{q}_1}(R_{\mathbf{q}}(\vec{\mathbf{v}})), R_{\mathbf{q}_2}(R_{\mathbf{q}}(\vec{\mathbf{v}}))) \\
&= \max_{\substack{\vec{\mathbf{v}}' = R_{\mathbf{q}}^{-1}(\vec{\mathbf{v}}), \\ \vec{\mathbf{v}}' \in S^2}} (R_{\mathbf{q}_1}(\vec{\mathbf{v}}'), R_{\mathbf{q}_2}(\vec{\mathbf{v}}')) \\
&= d_{SO(3)}(\mathbf{q}_1, \mathbf{q}_2)
\end{aligned} \tag{59}$$

by changing the variable.

The left multiplication distance-preserving property, i.e., Eq. (58), holds as

$$\begin{aligned}
d_{SO(3)}(\mathbf{q} \otimes \mathbf{q}_1, \mathbf{q} \otimes \mathbf{q}_2) &= \max_{\vec{\mathbf{v}} \in S^2} d_{S^2}(R_{\mathbf{q} \otimes \mathbf{q}_1}(\vec{\mathbf{v}}), R_{\mathbf{q} \otimes \mathbf{q}_2}(\vec{\mathbf{v}})) \\
&= \max_{\vec{\mathbf{v}} \in S^2} d_{S^2}(R_{\mathbf{q}}(R_{\mathbf{q}_1}(\vec{\mathbf{v}})), R_{\mathbf{q}}(R_{\mathbf{q}_2}(\vec{\mathbf{v}}))) \\
&= \max_{\vec{\mathbf{v}} \in S^2} d_{S^2}(R_{\mathbf{q}_1}(\vec{\mathbf{v}}), R_{\mathbf{q}_2}(\vec{\mathbf{v}})) \\
&= d_{SO(3)}(\mathbf{q}_1, \mathbf{q}_2)
\end{aligned} \tag{60}$$

because the distance on the unit sphere  $S^2$  has the following property

$$d_{S^2}(\vec{\mathbf{v}}_1, \vec{\mathbf{v}}_2) = d_{S^2}(R_{\mathbf{q}}(\vec{\mathbf{v}}_1), R_{\mathbf{q}}(\vec{\mathbf{v}}_2)), \forall R_{\mathbf{q}} \in SO(3) \tag{61}$$

because the spatial rotation preserves the inner product.

With the properties of the distance on  $SO(3)$  described in Eqs. (57) and (58), several properties can be derived as follows.

$$\begin{aligned}
d_{SO(3)}(\mathbf{q}_1, \mathbf{q}_2) &= d_{SO(3)}(\mathbf{q}_e, \mathbf{q}_1^{-1} \otimes \mathbf{q}_2) \\
&= d_{SO(3)}(\mathbf{q}_2^{-1} \otimes \mathbf{q}_1, \mathbf{q}_e)
\end{aligned} \tag{62}$$

holds for any  $R_{\mathbf{q}_1}, R_{\mathbf{q}_2} \in SO(3)$ , where  $\mathbf{q}_e$  represents the still rotation, i.e., the rotation that does not move any vector. Moreover,

$$d_{SO(3)}(\mathbf{q}_e, \mathbf{q}) = d_{SO(3)}(\mathbf{q}_e, \mathbf{q}_p^{-1} \otimes \mathbf{q} \otimes \mathbf{q}_p) \tag{63}$$

holds for any  $R_{\mathbf{q}}, R_{\mathbf{q}_p} \in SO(3)$ .

For any  $R_{\mathbf{q}} \in SO(3)$ , there exists a rotation  $R_{\mathbf{q}_p} \in SO(3)$  such that the corresponding rotation matrix of  $R_{\mathbf{q}_p^{-1} \otimes \mathbf{q} \otimes \mathbf{q}_p}$  is (Leon, 1986)

$$\begin{pmatrix} \cos\phi & -\sin\phi \\ \sin\phi & \cos\phi \\ 0 & 0 & 1 \end{pmatrix}, \tag{64}$$

where  $\phi$  is the rotation angle of  $R_{\mathbf{q}}$ . Thus, from Eqs. (62), (63), and (64), there exist  $R_{\mathbf{q}_p}$  and  $\phi \in [-\pi, \pi]$  such that

$$\begin{aligned}
d_{SO(3)}(\mathbf{q}_1, \mathbf{q}_2) &= d_{SO(3)}(\mathbf{q}_e, \mathbf{q}_1^{-1} \otimes \mathbf{q}_2) \\
&= d_{SO(3)}(\mathbf{q}_e, \mathbf{q}_p^{-1} \otimes \mathbf{q}_1^{-1} \otimes \mathbf{q}_2 \otimes \mathbf{q}_p),
\end{aligned} \tag{65}$$

where the corresponding rotation matrix of  $R_{\mathbf{q}_p^{-1} \otimes \mathbf{q}_1^{-1} \otimes \mathbf{q}_2 \otimes \mathbf{q}_p}$  is  $\begin{pmatrix} \cos\phi & -\sin\phi \\ \sin\phi & \cos\phi \\ 0 & 0 & 1 \end{pmatrix}$ , and  $\phi$  is the angle of rotation of  $R_{\mathbf{q}_1^{-1} \otimes \mathbf{q}_2}$ .

From the definition of the distance in  $S^2$ , i.e., Eq. (17), and the definition of the distance in  $SO(3)$ , i.e., Eq. (18), Eq. (65) is converted to

$$\begin{aligned}
d_{SO(3)}(\mathbf{q}_1, \mathbf{q}_2) &= \max_{(xyz) \in S^2} d_{S^2}((xyz), (\cos\phi - \sin\phi \sin\phi \cos\phi)(xyz)) \\
&= \max_{(xyz) \in S^2} d_{S^2}((xyz), (x \cos\phi - y \sin\phi \sin\phi + y \cos\phi z)) \\
&= \max_{(xyz) \in S^2} \cos^{-1}(x(x \cos\phi - y \sin\phi) + y(x \sin\phi + y \cos\phi) + z^2) \\
&= \max_{(xyz) \in S^2} \cos^{-1}((1 - z^2)\cos\phi + z^2) \\
&= \max_{t \in [0, 1]} \cos^{-1}((1 - t)\cos\phi + t) = |\phi|,
\end{aligned} \tag{66}$$

that has a ranges  $[0, \pi]$ . Therefore, the distance  $d_{SO(3)}(\mathbf{q}_1, \mathbf{q}_2)$  is equal to the angle of rotation of  $R_{\mathbf{q}_1^{-1} \otimes \mathbf{q}_2}$ .

In the second step, i.e., we show that  $2\cos^{-1}(|\mathbf{q}_1 \cdot \mathbf{q}_2|)$  in Eq. (19) is equal to the angle of rotation of  $R_{\mathbf{q}_1^{-1} \otimes \mathbf{q}_2}$ .

As the unit quaternion multiplication has this property (Conway and Smith, 2003)

$$(\mathbf{q} \otimes \mathbf{q}_1) \cdot (\mathbf{q} \otimes \mathbf{q}_2) = \mathbf{q} \cdot \mathbf{q}_2 \tag{67}$$

by selecting  $\mathbf{q} = \mathbf{q}_1^{-1}$ ,  $2\cos^{-1}(|\mathbf{q}_1 \cdot \mathbf{q}_2|)$  is derived into

$$\begin{aligned}
2\cos^{-1}(|\mathbf{q}_1 \cdot \mathbf{q}_2|) &= 2\cos^{-1}(|(\mathbf{q} \otimes \mathbf{q}_1) \cdot (\mathbf{q} \otimes \mathbf{q}_2)|) \\
&= 2\cos^{-1}(|(1, 0, 0, 0)^T \cdot (\mathbf{q}_1^{-1} \otimes \mathbf{q}_2)|).
\end{aligned} \tag{68}$$

Because the rotation angle of  $R_{\mathbf{q}_1^{-1} \otimes \mathbf{q}_2}$  is  $\phi$ , from Eq. (10),  $\mathbf{q}_1^{-1} \otimes \mathbf{q}_2 = \begin{pmatrix} \cos\frac{\phi}{2} \\ \sin\frac{\phi}{2}\hat{\mathbf{n}} \end{pmatrix}$  or  $\mathbf{q}_1^{-1} \otimes \mathbf{q}_2 = \begin{pmatrix} \cos\frac{-\phi}{2} \\ \sin\frac{-\phi}{2}\hat{\mathbf{n}} \end{pmatrix}$ , where the unit vector  $\hat{\mathbf{n}}$  is the rotation axis.

Thus, using Eq. (68), the second step is proven as follows

$$\begin{aligned}
2\cos^{-1}(|\mathbf{q}_1 \cdot \mathbf{q}_2|) &= 2\cos^{-1}(|(1, 0, 0, 0)^T \cdot (\mathbf{q}_1^{-1} \otimes \mathbf{q}_2)|) \\
&= 2\cos^{-1}\left(\left|\begin{pmatrix} 1 \\ 0 \\ 0 \\ 0 \end{pmatrix} \cdot \begin{pmatrix} \cos\frac{\pm\phi}{2} \\ \sin\frac{\pm\phi}{2}\hat{\mathbf{n}} \end{pmatrix}\right|\right) = |\phi|.
\end{aligned} \tag{69}$$

Hence, the distance  $d_{SO(3)}(R_{\mathbf{q}_1}, R_{\mathbf{q}_2})$  defined in Eq. (18) and  $2\cos^{-1}(|\mathbf{q}_1 \cdot \mathbf{q}_2|)$  in Eq. (19) are proven to be the rotation angles of  $R_{\mathbf{q}_1^{-1} \otimes \mathbf{q}_2}$ . Thus, Eq. (19) is equivalent to the distance definition Eq. (18).

Furthermore, we will prove that Eq. (20) is equivalent to Eq. (19). The proof is as follows.

$$\begin{aligned} 2 \cos^{-1} \left( 1 - \frac{\|\mathbf{q}_1 - \mathbf{q}_2\|^2}{2} \right) &= 2 \cos^{-1} \left( 1 - \frac{\|\mathbf{q}_1\|^2 + \|\mathbf{q}_2\|^2 - 2\mathbf{q}_1 \cdot \mathbf{q}_2}{2} \right) \\ &= 2 \cos^{-1} (\|\mathbf{q}_1 \cdot \mathbf{q}_2\|). \end{aligned} \quad (70)$$

Therefore, we have proven the equivalence between Eqs. (20), (19) and (18).

### E.3. Rotation distance as upper bound of direction change

In this section, we prove that for a 3D object rotated by two rotations  $R_{\mathbf{q}_1}$  and  $R_{\mathbf{q}_2}$ , the distance between the orientations represented by their projection direction, i.e.,  $\vec{\mathbf{v}}_{p_{\mathbf{q}_1}}$  and  $\vec{\mathbf{v}}_{p_{\mathbf{q}_2}}$ , is bounded above by the distance  $d_{SO(3)}(R_{\mathbf{q}_1}, R_{\mathbf{q}_2})$ .

Selecting  $\vec{\mathbf{v}}$  in Eq. (18) as  $\vec{\mathbf{v}}_n$  in Eq. (12),

$$\begin{aligned} d_{SO(3)}(\mathbf{q}_1, \mathbf{q}_2) &= \max_{\mathbf{v} \in S^2} d_S(R_{\mathbf{q}_1}(\vec{\mathbf{v}}), R_{\mathbf{q}_2}(\vec{\mathbf{v}})) \\ &\geq d_S(R_{\mathbf{q}_1}(\vec{\mathbf{v}}_n), R_{\mathbf{q}_2}(\vec{\mathbf{v}}_n)) \\ &= d_S(\vec{\mathbf{v}}_{p_{\mathbf{q}_1}}, \vec{\mathbf{v}}_{p_{\mathbf{q}_2}}). \end{aligned} \quad (71)$$

Thus, the distance between  $R_{\mathbf{q}_1}$  and  $R_{\mathbf{q}_2}$  is the upper bound of their projection direction difference.

## Appendix F. Scaled Euler angle method

In this section, the procedure of generating quasi-regular grid on  $S^2$  by scaled Euler angle method is introduced.

Recall that the rotation of the ZYZ Euler angles correspond to a unit quaternion given by Eq. (47). In these coordinates, the  $SO(3)$ -invariant measure of  $S^2$  is proportional to  $\sin\theta d\phi d\theta$  (Yershova et al., 2010). Therefore, such quasi-regular grid on  $S^2$  can be generated as follows.

The range of  $\theta$ , i.e.,  $[0, \pi]$  is equally partitioned at  $\frac{\pi}{N}$  interval.  $N$  is a positive integer, which controls the fineness of the grid. Therefore, the series of  $\theta$  of the grid is  $\{0, \frac{\pi}{N}, \dots, \pi\}$ . For the purpose of making grid spacing approximately equivalent, the series of  $\phi$  of the grid at some  $\theta$  partitions the range  $[0, 2\pi]$  into

$$[(2N-1)\sin\theta] + 1 \quad (72)$$

arcs. That is, some  $\theta$ , the series of  $\phi$  of the grid is  $\{0, \frac{2\pi}{[(2N-1)\sin\theta]+1}, \dots, 1 - \frac{2\pi}{[(2N-1)\sin\theta]+1}\}$ . A quasi-regular grid on  $S^2$  is generated at approximate  $\frac{\pi}{N}$  interval.

## Appendix G. Projective arithmetic mean as an approximation of geometric mean

In this section, the projective arithmetic mean will be proven to approximate the geometric mean for a given set of rotations  $\{R_{\mathbf{q}_i}\}_{1 \leq i \leq N}$  and their weights  $\{w_i\}_{1 \leq i \leq N}$ .

The projective arithmetic mean is defined by Oshman and Carmi (2006)

$$\arg \min_{R_{\mathbf{q}} \in SO(3)} \sum_{i=1}^N w_i \| \mathbf{M}_{\mathbf{q}} - \mathbf{M}_{\mathbf{q}_i} \|_F^2, \quad (73)$$

where  $\mathbf{M}_{\mathbf{q}}$  represents the rotation matrix of rotation  $R_{\mathbf{q}}$ , and  $\|\cdot\|_F$  represents the Frobenius norm (Horn, 1985).

We state that  $\|\mathbf{M}_{\mathbf{q}} - \mathbf{M}_{\mathbf{q}_i}\|_F$  is related to the distance defined in Eq. (18) (Moakher, 2002), such that

$$\|\mathbf{M}_{\mathbf{q}} - \mathbf{M}_{\mathbf{q}_i}\|_F = 2\sqrt{2} \sin \frac{d_{SO(3)}(\mathbf{q}, \mathbf{q}_i)}{2}. \quad (74)$$

Eq. (74) can be proven as follows. From E.2 as Eqs. (65) and (66), there exist  $R_{\mathbf{q}_p}$  and  $\phi \in [-\pi, \pi]$  such that

$$d_{SO(3)}(\mathbf{q}, \mathbf{q}_i) = d_{SO(3)}(\mathbf{q}_e, \mathbf{q}_p^{-1} \otimes \mathbf{q}^{-1} \otimes \mathbf{q}_i \otimes \mathbf{q}_p), \quad (75)$$

where the corresponding rotation matrix of  $R_{\mathbf{q}_p^{-1} \otimes \mathbf{q}^{-1} \otimes \mathbf{q}_i \otimes \mathbf{q}_p}$  is  $\mathbf{M}_{\mathbf{q}_p^{-1} \otimes \mathbf{q}^{-1} \otimes \mathbf{q}_i \otimes \mathbf{q}_p} = \begin{pmatrix} \cos\phi & -\sin\phi & & \\ \sin\phi & \cos\phi & & \\ & & 1 & \\ & & & \end{pmatrix}$ , and  $d_{SO(3)}(\mathbf{q}, \mathbf{q}_i) = |\phi|$ . Moreover, Frobenius norm of matrices is invariant under rotations (Leon, 1986), i.e.,

$$\|\mathbf{A}\|_F = \|\mathbf{MA}\|_F = \|\mathbf{AM}\|_F \quad (76)$$

holds for any matrix  $\mathbf{A}$  and rotation  $\mathbf{M}$ . Thus,

$$\begin{aligned}
\|\mathbf{M}_q - \mathbf{M}_{q_l}\|_F &= \|\mathbf{M}_q^{-1} \mathbf{M}_q - \mathbf{M}_q^{-1} \mathbf{M}_{q_l}\|_F \\
&= \|\mathbf{I} - \mathbf{M}_{q^{-1} \otimes q_l}\|_F \\
&= \|\mathbf{M}_{q_p} - \mathbf{M}_{q^{-1} \otimes q_l} \mathbf{M}_{q_p}\|_F \\
&= \|\mathbf{M}_{q_p}^{-1} \mathbf{M}_{q_p} - \mathbf{M}_{q_p}^{-1} \mathbf{M}_{q^{-1} \otimes q_l} \mathbf{M}_{q_p}\|_F \\
&= \|\mathbf{I} - \mathbf{M}_{q_p^{-1} \otimes q^{-1} \otimes q_l \otimes q_p}\|_F \\
&= \left\| \begin{pmatrix} 1 & & \\ & 1 & \\ & & 1 \end{pmatrix} - \begin{pmatrix} \cos \phi & -\sin \phi & \\ \sin \phi & \cos \phi & \\ & & 1 \end{pmatrix} \right\|_F \\
&= \left\| \begin{pmatrix} 1 - \cos \phi & \sin \phi & \\ -\sin \phi & 1 - \cos \phi & \\ & & 0 \end{pmatrix} \right\|_F \\
&= \sqrt{2(1 - \cos \phi)^2 + 2 \sin^2 \phi} \\
&= \sqrt{4 - 4 \cos \phi} \\
&= 2\sqrt{2 \sin^2 \frac{\phi}{2}} \\
&= 2\sqrt{2} \sin \frac{|\phi|}{2} \\
&= 2\sqrt{2} \sin \frac{d_{SO(3)}(\mathbf{q}, \mathbf{q}_l)}{2}.
\end{aligned} \tag{77}$$

Thus, we have proven that Eq. (74) holds.

Therefore, because  $f(x) = 2\sqrt{2} \sin \frac{x}{2}$  is a monotonic increasing function where  $x$  ranges  $[0, \pi]$ , the projective arithmetic mean approximates the geometric mean to some degree.

#### Appendix H. Selection of covariance matrix that causes the ACG distribution to reach a maximum probability density at a given unit quaternion

In this section, we introduce a suitable method for selecting the covariance matrix  $\mathbf{A}$  in the ACG distribution to aid the  $ACG(\mathbf{A})$  attain a maximum probability density at some unit quaternion  $\mathbf{q}$ . As stated in Section 5.2.1,  $\mathbf{A}$  is a positive-definite symmetric matrix with  $\mathbf{q}$  as the principal

eigenvector. Assuming  $\mathbf{q} = \begin{pmatrix} q_0 \\ q_1 \\ q_2 \\ q_3 \end{pmatrix}$ , we can select  $\mathbf{A}$  as

$$\mathbf{A} = \mathbf{P} \begin{pmatrix} k^2 & & & \\ & 1 & & \\ & & 1 & \\ & & & 1 \end{pmatrix} \mathbf{P}^T, \tag{78}$$

where

$$\mathbf{P} = \begin{pmatrix} q_0 & -q_1 & -q_2 & -q_3 \\ q_1 & q_0 & -q_3 & q_2 \\ q_2 & q_3 & q_0 & -q_1 \\ q_3 & -q_2 & q_1 & q_0 \end{pmatrix} \tag{79}$$

is an orthogonal matrix and  $k > 1$ .

$\mathbf{A}^T = \mathbf{P} \begin{pmatrix} k^2 & & & \\ & 1 & & \\ & & 1 & \\ & & & 1 \end{pmatrix} \mathbf{P}^T = \mathbf{A}$ ,  $\mathbf{A}$  is symmetric. Moreover, because  $k > 1$ , from the principle of eigenvalue decomposition (Leon, 1986),  $\mathbf{q}$  is the principal eigenvector of  $\mathbf{A}$ .

#### Appendix I. Probability density of unit vector generated by rotations with ACG distribution

In this section, we discuss the distribution of a unit vector rotated by rotations sampled from an ACG distribution with a special covariance matrix  $\mathbf{A} = \begin{pmatrix} k^2 & & & \\ & 1 & & \\ & & 1 & \\ & & & 1 \end{pmatrix}$ , where  $k > 1$ . For a vector  $\mathbf{v}_0$  and a unit quaternion  $\mathbf{q}$  sampled from  $ACG(\mathbf{A})$ , the rotated vector  $\vec{\mathbf{v}}$  is calculated using  $\vec{\mathbf{v}} = R_q(\vec{\mathbf{v}}_0) = \mathbf{q} \otimes \begin{pmatrix} 0 \\ \mathbf{v}_0 \end{pmatrix} \otimes \mathbf{q}^T$ . We denote the probability density of this distribution of  $\vec{\mathbf{v}}$  by  $p(\vec{\mathbf{v}}; \vec{\mathbf{v}}_0, \mathbf{A})$ .

The concept of the deviation of  $p(\vec{\mathbf{v}}; \vec{\mathbf{v}}_0, \mathbf{A})$  uses the principle of marginal probability density, such that

$$p(\vec{\mathbf{v}}; \vec{\mathbf{v}}_0, \mathbf{A}) d\vec{\mathbf{v}} = \int_{\{\mathbf{q} | \mathbf{q} \otimes \begin{pmatrix} 0 \\ \mathbf{v}_0 \end{pmatrix} \otimes \mathbf{q}^T = \vec{\mathbf{v}}\}} p(\mathbf{q}; \mathbf{A}) d\mathbf{q}. \tag{80}$$

We will prove that  $p(\vec{\mathbf{v}}; \vec{\mathbf{v}}_0, \mathbf{A})$  can be calculated as

$$p(\vec{\mathbf{v}}; \vec{\mathbf{v}}_0, \mathbf{A}) = \frac{1}{2\sqrt{2}k} \frac{(\frac{1}{k^2} - 1)\cos\theta + (\frac{1}{k^2} + 3)}{((\frac{1}{k^2} - 1)\cos\theta + (\frac{1}{k^2} + 1))^{\frac{3}{2}}}, \quad (81)$$

where  $\cos\theta = \vec{\mathbf{v}} \cdot \vec{\mathbf{v}}_0$ , i.e.,  $\theta$  is the angular distance between  $\vec{\mathbf{v}}$  and  $\vec{\mathbf{v}}_0$ . From Eq. (81), we can also conclude that  $\vec{\mathbf{v}} = R_{\mathbf{q}}(\vec{\mathbf{v}}_0)$  follows a distribution invariant under rotation about  $\vec{\mathbf{v}}_0$ . Moreover, by converting Eq. (81) to

$$p(\vec{\mathbf{v}}; \vec{\mathbf{v}}_0, \mathbf{A}) = \frac{1}{2\sqrt{2}k} \left( \frac{1}{((\frac{1}{k^2} - 1)\cos\theta + (\frac{1}{k^2} + 1))^{\frac{1}{2}}} + \frac{2}{((\frac{1}{k^2} - 1)\cos\theta + (\frac{1}{k^2} + 1))^{\frac{3}{2}}} \right), \quad (82)$$

we can conclude that  $p(\vec{\mathbf{v}}'; \vec{\mathbf{v}}_0; \mathbf{A})$  monotonically decreases with increasing  $\theta$  for  $k > 1$ , that is  $p(\vec{\mathbf{v}}; \vec{\mathbf{v}}_0, \mathbf{A})$ , i.e., the probability density of  $\vec{\mathbf{v}}$  reaches a maximum at  $\vec{\mathbf{v}}_0$ .

In the first part of this proof, we will specify  $\vec{\mathbf{v}}_0$  to be  $(0, 0, 1)^T$  and prove the above statement. In the second part of this proof, although we will extend  $\vec{\mathbf{v}}_0$  from  $(0, 0, 1)^T$  to an arbitrary unit vector, the above statement will still hold.

For the first part,  $\vec{\mathbf{v}}_0 = (0, 0, 1)^T$ . We use the Euler angles to parameterize spatial rotations. Considering ZYZ proper Euler angles  $\phi$ ,  $\theta$ , and  $\psi$ , where  $\phi \in [0, 2\pi)$ ,  $\theta \in [0, \pi]$ , and  $\psi \in [0, 2\pi)$ , the rotation  $R_{\phi, \theta, \psi}$  is given by

$$R_{\phi, \theta, \psi} = \begin{pmatrix} c_3 & -s_3 \\ s_3 & c_3 \\ 0 & 0 \end{pmatrix} \begin{pmatrix} c_2 & s_2 \\ -s_2 & c_2 \\ 0 & 0 \end{pmatrix} \begin{pmatrix} c_1 & -s_1 \\ s_1 & c_1 \\ 0 & 0 \end{pmatrix} = \begin{pmatrix} c_3 c_2 c_1 - s_3 s_1 & -c_3 c_2 s_1 - s_3 c_1 & c_3 s_2 \\ s_3 c_2 c_1 + c_3 s_1 & -s_3 c_2 s_1 + c_3 c_1 & s_3 s_2 \\ -s_2 c_1 & s_2 s_1 & c_2 \end{pmatrix} \quad (83)$$

$$c_1 = \cos\phi,$$

$$s_1 = \sin\phi,$$

where  $c_2 = \cos\theta$ , and  $s_2 = \sin\theta$ . Let  $R_{\phi, \theta, \psi}$  act on  $\vec{\mathbf{v}}_0 = (0, 0, 1)^T$ ,

$$\vec{\mathbf{v}} = R_{\phi, \theta, \psi}(\vec{\mathbf{v}}_0) = \begin{pmatrix} c_3 s_2 \\ s_3 s_2 \\ c_2 \end{pmatrix} = \begin{pmatrix} \sin\theta \cos\psi \\ \sin\theta \sin\psi \\ \cos\theta \end{pmatrix} \quad (84)$$

we observe that  $\vec{\mathbf{v}} = R_{\mathbf{q}}(\vec{\mathbf{v}}_0)$  is independent of  $\phi$ . That is,  $\vec{\mathbf{v}} = R_{\mathbf{q}}(\vec{\mathbf{v}}_0)$  follows a distribution invariant under rotation about  $\vec{\mathbf{v}}_0 = (0, 0, 1)^T$ .

Recall that the rotation of ZYZ Euler angles corresponds to a unit quaternion given by Eq. (47), and the Haar measure under these coordinates is  $d\mathbf{q}_{\phi, \theta, \psi} = \frac{\sin\theta}{8\pi^2} d\phi d\theta d\psi$  (Yershova et al., 2010). Therefore, from the ACG probability density function described in Eq. (33), the probability density of the ACG distribution using Euler angles is

$$\begin{aligned} & p(\mathbf{q}_{\phi, \theta, \psi}; \mathbf{A}) d\mathbf{q}_{\phi, \theta, \psi} \\ &= |\mathbf{A}|^{-\frac{1}{2}} (\mathbf{q}_{\phi, \theta, \psi}^T \mathbf{A}^{-1} \mathbf{q}_{\phi, \theta, \psi})^{-\frac{2\sin\theta}{8\pi^2}} d\phi d\theta d\psi \\ &= \frac{1}{k(\frac{1}{k^2} \cos^2 \frac{\theta}{2} \cos^2 \frac{\psi+\phi}{2} + \sin^2 \frac{\theta}{2} \sin^2 \frac{\psi-\phi}{2} + \sin^2 \frac{\theta}{2} \cos^2 \frac{\psi-\phi}{2} + \cos^2 \frac{\theta}{2} \sin^2 \frac{\psi+\phi}{2})^2} \cdot \frac{\sin\theta}{8\pi^2} d\phi d\theta d\psi \\ &= \frac{1}{k(\frac{1}{k^2} \cos^2 \frac{\theta}{2} \cos^2 \frac{\psi+\phi}{2} + \sin^2 \frac{\theta}{2} + \cos^2 \frac{\theta}{2} \sin^2 \frac{\psi+\phi}{2})^2} \cdot \frac{\sin\theta}{8\pi^2} d\phi d\theta d\psi \end{aligned} \quad (85)$$

where  $p(\mathbf{q}_{\phi, \theta, \psi}; \mathbf{A})$  is the probability density of the ACG distribution with covariance matrix  $\mathbf{A}$ .

By substituting Eq. (85) into (80),

$$\begin{aligned}
& p(\vec{\mathbf{v}}; \vec{\mathbf{v}}_0, \mathbf{A}) d\vec{\mathbf{v}} \\
&= p(\vec{\mathbf{v}}_{\psi, \theta}; \vec{\mathbf{v}}_0, \mathbf{A}) d\vec{\mathbf{v}}_{\psi, \theta} \\
&= \int_{\left\{ \mathbf{q} | \mathbf{q} \otimes \begin{pmatrix} 0 \\ \vec{\mathbf{v}}_0 \end{pmatrix} \otimes \mathbf{q}^* = \vec{\mathbf{v}}'_{\psi, \theta} \right\}} p(\mathbf{q}_{\psi, \theta}; \mathbf{A}) d\mathbf{q}_{\psi, \theta, \psi} \\
&= \int_{\phi=0}^{2\pi} p(\mathbf{q}_{\psi, \theta, \phi}; \mathbf{A}) d\mathbf{q}_{\psi, \theta, \phi} \\
&= \int_{\phi=0}^{2\pi} \frac{1}{k(\frac{1}{k^2} \cos^2 \frac{\theta}{2} \cos^2 \frac{\psi+\phi}{2} + \sin^2 \frac{\theta}{2} + \cos^2 \frac{\theta}{2} \sin^2 \frac{\psi+\phi}{2})^2} \cdot \frac{\sin \theta}{8\pi^2} d\psi d\theta d\phi \\
&= \frac{\sin \theta}{2k\pi^2} \int_{\phi=0}^{2\pi} \frac{1}{(\frac{1}{k^2} \cos^2 \frac{\theta}{2} (1 + \cos(\psi + \phi)) + 2 \sin^2 \frac{\theta}{2} + \cos^2 \frac{\theta}{2} (1 - \cos(\psi + \phi)))^2} d\psi d\theta d\phi \\
&= \frac{\sin \theta}{2k\pi^2} \int_{\phi=0}^{2\pi} \frac{1}{(\frac{1}{k^2} \cos^2 \frac{\theta}{2} (1 + \cos \phi) + 2 \sin^2 \frac{\theta}{2} + \cos^2 \frac{\theta}{2} (1 - \cos \phi))^2} d\psi d\theta d\phi \\
&= \frac{\sin \theta}{2k\pi^2} \int_{\phi=0}^{2\pi} \frac{1}{((\frac{1}{k^2} - 1) \cos^2 \frac{\theta}{2} \cos \phi + (\frac{1}{k^2} + 1) \cos^2 \frac{\theta}{2} + 2 \sin^2 \frac{\theta}{2})^2} d\psi d\theta d\phi \\
&= \frac{\sin \theta}{2k\pi^2} \frac{2\pi((\frac{1}{k^2} + 1) \cos^2 \frac{\theta}{2} + 2 \sin^2 \frac{\theta}{2})}{((\frac{1}{k^2} + 1) \cos^2 \frac{\theta}{2} + 2 \sin^2 \frac{\theta}{2})^2 - ((\frac{1}{k^2} - 1)^2 \cos^4 \frac{\theta}{2})^2} d\psi d\theta \\
&= \frac{\sin \theta}{k\pi} \frac{(\frac{1}{k^2} + 1) \cos^2 \frac{\theta}{2} + 2 \sin^2 \frac{\theta}{2}}{(4(\frac{1}{k^2} \cos^4 \frac{\theta}{2} + 4(\frac{1}{k^2} + 1) \cos^2 \frac{\theta}{2} \sin^2 \frac{\theta}{2} + 4 \sin^4 \frac{\theta}{2})^{\frac{3}{2}}} d\psi d\theta \\
&= \frac{\sin \theta}{2k\pi} \frac{(\frac{1}{k^2} + 1)(1 + \cos \theta) + 2(1 - \cos \theta)}{(\frac{1}{k^2}(1 + \cos \theta)^2 + (\frac{1}{k^2} + 1)(1 + \cos \theta)(1 - \cos \theta) + (1 - \cos \theta)^2)^{\frac{3}{2}}} d\psi d\theta \\
&= \frac{\sin \theta}{4\sqrt{2}k\pi} \frac{(\frac{1}{k^2} - 1)\cos \theta + (\frac{1}{k^2} + 3)}{((\frac{1}{k^2} - 1)\cos \theta + (\frac{1}{k^2} + 1))^{\frac{3}{2}}} d\psi d\theta
\end{aligned} \tag{86}$$

In  $S^2$ ,  $d\vec{\mathbf{v}}_{\psi, \theta} = \frac{\sin \theta}{2\pi} d\psi d\theta$ . Thus,

$$p(\vec{\mathbf{v}}_{\psi, \theta}; \vec{\mathbf{v}}_0, \mathbf{A}) = \frac{1}{2\sqrt{2}k} \frac{(\frac{1}{k^2} - 1)\cos \theta + (\frac{1}{k^2} + 3)}{((\frac{1}{k^2} - 1)\cos \theta + (\frac{1}{k^2} + 1))^{\frac{3}{2}}} \tag{87}$$

Therefore, we have proven Eq. (81) for  $\vec{\mathbf{v}} = (0, 0, 1)^T$ .

In the second part, although we extend  $\vec{\mathbf{v}}_0$  from  $(0, 0, 1)^T$  to an arbitrary unit vector, the above statement holds. Suppose  $\vec{\mathbf{v}}_0 = R_{\mathbf{q}_{\vec{\mathbf{v}}_0}} \begin{pmatrix} 0 \\ 0 \\ 1 \end{pmatrix}$ , that is,

$$\begin{aligned}
\begin{pmatrix} 0 \\ \vec{\mathbf{v}}_0 \end{pmatrix} &= \mathbf{q}_{\vec{\mathbf{v}}_0} \otimes \begin{pmatrix} 0 \\ 0 \\ 0 \end{pmatrix} \otimes \mathbf{q}_{\vec{\mathbf{v}}_0}^*, \text{ then Eq. (80) can be derived by} \\
p(\vec{\mathbf{v}}; \vec{\mathbf{v}}_0, \mathbf{A}) d\vec{\mathbf{v}}^1 &= \int_{\left\{ \mathbf{q} | \mathbf{q} \otimes \begin{pmatrix} 0 \\ \vec{\mathbf{v}}_0 \end{pmatrix} \otimes \mathbf{q}^* = \vec{\mathbf{v}} \right\}} p(\mathbf{q}; \mathbf{A}) d\mathbf{q} \\
&= \int_{\left\{ \mathbf{q} | \mathbf{q} \otimes \mathbf{q}_{\vec{\mathbf{v}}_0} \otimes \begin{pmatrix} 0 \\ 0 \\ 0 \end{pmatrix} \otimes \mathbf{q}_{\vec{\mathbf{v}}_0}^* \otimes \mathbf{q}^* = \vec{\mathbf{v}} \right\}} p(\mathbf{q}; \mathbf{A}) d\mathbf{q} \\
&= \int_{\left\{ \mathbf{q} | \mathbf{q} \otimes \mathbf{q}_{\vec{\mathbf{v}}_0} \otimes \begin{pmatrix} 0 \\ 0 \\ 0 \end{pmatrix} \otimes \mathbf{q}_{\vec{\mathbf{v}}_0}^* \otimes \mathbf{q}^* = \mathbf{q}_{\vec{\mathbf{v}}_0} \otimes \vec{\mathbf{v}}' \otimes \mathbf{q}_{\vec{\mathbf{v}}_0}^* \right\}} p(\mathbf{q}; \mathbf{A}) d\mathbf{q} \\
&= \int_{\left\{ \mathbf{q} | \mathbf{q}_{\vec{\mathbf{v}}_0}^* \otimes \mathbf{q} \otimes \mathbf{q}_{\vec{\mathbf{v}}_0} \otimes \begin{pmatrix} 0 \\ 0 \\ 0 \end{pmatrix} \otimes \mathbf{q}_{\vec{\mathbf{v}}_0}^* \otimes \mathbf{q}^* \otimes \mathbf{q}_{\vec{\mathbf{v}}_0}^* = \vec{\mathbf{v}}' \right\}} p(\mathbf{q}; \mathbf{A}) d\mathbf{q} \\
&= \int_{\left\{ \mathbf{q} | \mathbf{q} \otimes \begin{pmatrix} 0 \\ 0 \\ 0 \end{pmatrix} \otimes \mathbf{q}^* = \vec{\mathbf{v}}' \right\}} p(\mathbf{q}_{\vec{\mathbf{v}}_0} \otimes \mathbf{q} \otimes \mathbf{q}_{\vec{\mathbf{v}}_0}^*; \mathbf{A}) d(\mathbf{q}_{\vec{\mathbf{v}}_0} \otimes \mathbf{q} \otimes \mathbf{q}_{\vec{\mathbf{v}}_0}^*) \\
&= \int_{\left\{ \mathbf{q} | \mathbf{q} \otimes \begin{pmatrix} 0 \\ 0 \\ 0 \end{pmatrix} \otimes \mathbf{q}^* = \vec{\mathbf{v}}' \right\}} p(\mathbf{q}'; \mathbf{A}) d\mathbf{q}' ,
\end{aligned} \tag{88}$$

where  $\vec{\mathbf{v}} = R_{\mathbf{q}_{\vec{\mathbf{v}}_0}}(\vec{\mathbf{v}}')$  and  $\mathbf{q}' = \mathbf{q}_{\vec{\mathbf{v}}_0} \otimes \mathbf{q} \otimes \mathbf{q}_{\vec{\mathbf{v}}_0}^*$ .

Note that  $d\mathbf{q}$  is the Haar measure on  $S^3$ , hence (Nachbin, 1965)

$$d\mathbf{q} = d\mathbf{q}'.$$

Moreover,

$$\tag{89}$$

$$\begin{aligned}
p(\mathbf{q}; \mathbf{A}) &= |\mathbf{A}|^{-\frac{1}{2}} (\mathbf{q}^T \mathbf{A}^{-1} \mathbf{q})^{-2} \\
&= \frac{1}{k} \left( \left( q_0, \vec{\mathbf{n}}_q^T \right) \begin{pmatrix} \frac{1}{k^2} & \\ & \mathbf{I} \end{pmatrix} \begin{pmatrix} q_0 \\ \vec{\mathbf{n}}_q \end{pmatrix} \right)^{-2} \\
&= \frac{1}{k} \left( \left( q_0, \vec{\mathbf{n}}_q^T \right) \begin{pmatrix} \frac{q_0}{k^2} \\ \vec{\mathbf{n}}_q \end{pmatrix} \right)^{-2} \\
&= \frac{1}{k} \left( \frac{q_0^2}{k^2} + |\vec{\mathbf{n}}_q|^2 \right)^{-2}, 
\end{aligned} \tag{90}$$

where  $\mathbf{q} = \begin{pmatrix} q_0 \\ \vec{\mathbf{n}}_q \end{pmatrix}$ . Because

$$\begin{aligned}
\mathbf{q}' &= \mathbf{q}_{\vec{\mathbf{v}}_0} \otimes \mathbf{q} \otimes \mathbf{q}_{\vec{\mathbf{v}}_0}^* \\
&= \mathbf{q}_{\vec{\mathbf{v}}_0} \otimes \begin{pmatrix} q_0 \\ \vec{\mathbf{n}}_q \end{pmatrix} \otimes \mathbf{q}_{\vec{\mathbf{v}}_0}^* \\
&= \mathbf{q}_{\vec{\mathbf{v}}_0} \otimes \left( \begin{pmatrix} q_0 \\ 0 \end{pmatrix} + \begin{pmatrix} 0 \\ \vec{\mathbf{n}}_q \end{pmatrix} \right) \otimes \mathbf{q}_{\vec{\mathbf{v}}_0}^* \\
&= q_0 \mathbf{q}_{\vec{\mathbf{v}}_0} \otimes \mathbf{q}_{\vec{\mathbf{v}}_0}^* + \mathbf{q}_{\vec{\mathbf{v}}_0} \begin{pmatrix} 0 \\ \vec{\mathbf{n}}_q \end{pmatrix} \mathbf{q}_{\vec{\mathbf{v}}_0}^* \\
&= \begin{pmatrix} q_0 \\ R_{q_0}(\vec{\mathbf{n}}_q) \end{pmatrix}
\end{aligned} \tag{91}$$

and  $\mathbf{q}' = \begin{pmatrix} q'_0 \\ \vec{\mathbf{n}}'_q \end{pmatrix}$ , we have  $R_{\mathbf{q}_{\vec{\mathbf{v}}_0}}(\vec{\mathbf{n}}_q) = \vec{\mathbf{n}}'_q$ . In addition,  $R_{\mathbf{q}_{\vec{\mathbf{v}}_0}}$  is a spatial rotation,  $|\vec{\mathbf{n}}_q| = |\vec{\mathbf{n}}'_q|$ . Thus, from Eq. (80)  $p(\mathbf{q}; \mathbf{A}) = p(\mathbf{q}', \mathbf{A})$ .

By substituting Eqs. (89) and (92) into Eq. (88), we have

$$\begin{aligned}
p(\vec{\mathbf{v}}; \vec{\mathbf{v}}_0, \mathbf{A}) d\vec{\mathbf{v}} &= \int_{\left\{ \mathbf{q} | \mathbf{q} \otimes \begin{pmatrix} 0 \\ 0 \\ 1 \end{pmatrix} \otimes \mathbf{q}^* = \vec{\mathbf{v}} \right\}} p(\mathbf{q}; \mathbf{A}) d\mathbf{q}' \\
&= \int_{\left\{ \mathbf{q} | \mathbf{q} \otimes \begin{pmatrix} 0 \\ 0 \\ 1 \end{pmatrix} \otimes \mathbf{q}^* = \vec{\mathbf{v}}' \right\}} p(\mathbf{q}; \mathbf{A}) d\mathbf{q} \\
&= p(\vec{\mathbf{v}}'; (0, 0, 1)^T, \mathbf{A}) d\vec{\mathbf{v}}',
\end{aligned} \tag{93}$$

where  $\vec{\mathbf{v}} = R_{\mathbf{q}_{\vec{\mathbf{v}}_0}}(\vec{\mathbf{v}}')$ . Furthermore,

$$\vec{\mathbf{v}} \cdot \vec{\mathbf{v}}_0 = R_{\mathbf{q}_{\vec{\mathbf{v}}_0}}(\vec{\mathbf{v}}') \cdot \vec{\mathbf{v}}_0 = \vec{\mathbf{v}}' \cdot R_{\mathbf{q}_{\vec{\mathbf{v}}_0}^*}(\vec{\mathbf{v}}_0) = \vec{\mathbf{v}}' \cdot \begin{pmatrix} 0 \\ 0 \\ 1 \end{pmatrix} \tag{94}$$

and  $d\vec{\mathbf{v}} = d\vec{\mathbf{v}}'$ , thus Eq. (87) gives

$$\begin{aligned}
&p(\vec{\mathbf{v}}; \vec{\mathbf{v}}_0, \mathbf{A}) \\
&= p(\vec{\mathbf{v}}'; (0, 0, 1)^T, \mathbf{A}) \\
&= \frac{1}{2\sqrt{2}k} \frac{\left(\frac{1}{k^2} - 1\right)(\vec{\mathbf{v}}' \cdot (0, 0, 1)^T) + \left(\frac{1}{k^2} + 3\right)}{\left(\left(\frac{1}{k^2} - 1\right)(\vec{\mathbf{v}}' \cdot (0, 0, 1)^T) + \left(\frac{1}{k^2} + 1\right)\right)^{\frac{3}{2}}} \\
&= \frac{1}{2\sqrt{2}k} \frac{\left(\frac{1}{k^2} - 1\right)(\vec{\mathbf{v}} \cdot \vec{\mathbf{v}}_0) + \left(\frac{1}{k^2} + 3\right)}{\left(\left(\frac{1}{k^2} - 1\right)(\vec{\mathbf{v}} \cdot \vec{\mathbf{v}}_0) + \left(\frac{1}{k^2} + 1\right)\right)^{\frac{3}{2}}} \\
&= \frac{1}{2\sqrt{2}k} \frac{\left(\frac{1}{k^2} - 1\right)\cos\theta + \left(\frac{1}{k^2} + 3\right)}{\left(\left(\frac{1}{k^2} - 1\right)\cos\theta + \left(\frac{1}{k^2} + 1\right)\right)^{\frac{3}{2}}},
\end{aligned} \tag{95}$$

where  $\cos\theta = \vec{\mathbf{v}} \cdot \vec{\mathbf{v}}_0$ . Therefore, we have proven that Eq. (81) still holds if  $\vec{\mathbf{v}}$  is an arbitrary unit vector.

#### Appendix J. Confidence area of a unit vector rotated from ACG distribution with a special covariance matrix

In this section, we use the assumptions and notations in I. We prove that the method employed to calculate the confidence area using Eq. (39) holds.

Because  $\vec{\mathbf{v}}$  is in  $S^2$ , this implies  $\int_{\{\vec{\mathbf{v}} | \vec{\mathbf{v}} \cdot \vec{\mathbf{v}}_0 \in [-1, 1]\}} p(\vec{\mathbf{v}}; \vec{\mathbf{v}}_0, \mathbf{A}) d\vec{\mathbf{v}} = 1$ , Eq. (38) is equivalent to

$$\int_{\{\vec{\mathbf{v}} | \vec{\mathbf{v}} \cdot \vec{\mathbf{v}}_0 \in [-1, z_0]\}} p(\vec{\mathbf{v}}; \vec{\mathbf{v}}_0, \mathbf{A}) d\vec{\mathbf{v}} = 1 - a. \tag{96}$$

By substituting Eq. (37) into Eq. (96),

$$\begin{aligned}
1 - a &= \int_{\{\vec{\mathbf{v}} \mid \vec{\mathbf{v}} \cdot \vec{\mathbf{v}}_0 \in [-1, z_0]\}} p(\vec{\mathbf{v}}; \vec{\mathbf{v}}_0, \mathbf{A}) d\vec{\mathbf{v}} \\
&= \int_{\theta \in [\cos^{-1}(z_0), \pi]} \frac{1}{\sqrt{2}k} \frac{\left(\frac{1}{k^2} - 1\right)\cos\theta + \left(\frac{1}{k^2} + 1\right)}{\left(\left(\frac{1}{k^2} - 1\right)\cos\theta + \left(\frac{1}{k^2} + 1\right)\right)^{\frac{3}{2}}} \left( \frac{\sin\theta}{4\pi} d\theta \right) \\
&= \frac{k}{\sqrt{2}(1-k^2)} \left( \sqrt{\left(\frac{1}{k^2} - 1\right)z + \left(\frac{1}{k^2} + 1\right)} - \frac{2}{\sqrt{\left(\frac{1}{k^2} - 1\right)z + \left(\frac{1}{k^2} + 1\right)}} \right) \Big|_{z=-1}^{z_0} \\
&= \frac{k}{\sqrt{2}(1-k^2)} \left( \sqrt{\left(\frac{1}{k^2} - 1\right)z_0 + \left(\frac{1}{k^2} + 1\right)} - \frac{2}{\sqrt{\left(\frac{1}{k^2} - 1\right)z_0 + \left(\frac{1}{k^2} + 1\right)}} \right).
\end{aligned} \tag{97}$$

For simplicity, we denote  $\sqrt{\left(\frac{1}{k^2} - 1\right)z_0 + \left(\frac{1}{k^2} + 1\right)}$  by  $z'_0$  and  $\frac{\sqrt{2}(1-k^2)(1-a)}{k}$  by  $a'$ ; thus,

$$z'_0 - \frac{2}{z'_0} = a'. \tag{98}$$

$z'_0$  is the positive solution of  $z'_0 - \frac{2}{z'_0} = a'$ , as in

$$z'_0 = \frac{a' + \sqrt{a'^2 + 8}}{2} \tag{99}$$

wherein  $z_0$  can be determined by

$$z_0 = \frac{z'_0^2 - \left(\frac{1}{k^2} + 1\right)}{\frac{1}{k^2} - 1}. \tag{100}$$

Therefore, we have proven that the method employed to calculate the confidence area using Eq. (39) holds.

#### Appendix K. Approximation formula used to calculate confidence area of a unit vector rotated by rotations from ACG distribution using a special covariance matrix

In this section, we still use the assumptions and notations in Appendices I and J. We prove that the reciprocal of angular precision, i.e.,  $\frac{1}{\epsilon}$ , is asymptotically linear to  $k$ , and that the asymptote is

$$\frac{1-a}{2\sqrt{2a-a^2}}k \tag{101}$$

where  $\frac{1}{\epsilon}$  approaches if  $k \rightarrow \infty$ .

The proof is as follows. From Eq. (39), it can be seen that

$$z_0 = (1-k^2)(1-a)^2 - 1 + (1-a)\sqrt{(1-k^2)^2(1-a)^2 + 4k^2} \tag{102}$$

Note that if  $k \rightarrow \infty$ ,

$$\begin{aligned}
z_0 &= -1 + (1-k^2)(1-a)^2 \left( 1 - \sqrt{1 + \frac{4k^2}{(1-k^2)^2(1-a)^2}} \right) \\
&= -1 + (1-k^2)(1-a)^2 \left( 1 - 1 - \frac{2k^2}{(1-k^2)^2(1-a)^2} \right. \\
&\quad \left. + \frac{2k^4}{(1-k^2)^4(1-a)^4} + O(k^{-6}) \right) \\
&= -1 - \frac{2k^2}{1-k^2} + \frac{2k^4}{(1-k^2)^3(1-a)^2} + O(k^{-4}) \\
&= -1 + \frac{2}{1-k^2} - \frac{2k^{-2}}{(1-a)^2(1-k^{-2})^3} + O(k^{-4}) \\
&= -1 + 2(1+k^{-2} + O(k^{-4})) \\
&\quad - \frac{2}{(1-a)^2} k^{-2} (1 + O(k^{-2}))^3 + O(k^{-4}) \\
&= 1 + 2k^{-2} - \frac{2}{(1-a)^2} k^{-2} + O(k^{-4}) \\
&= 1 - \left( \frac{2}{(1-a)^2} - 2 \right) k^{-2} + O(k^{-4}) \\
&\rightarrow 1.
\end{aligned} \tag{103}$$

Hence,  $\theta_0 \rightarrow 0$  and  $\frac{1}{\epsilon} \rightarrow \infty$ . We aim to show that if  $k \rightarrow \infty$ ,  $\frac{1}{\epsilon}$  grows linearly in  $k$ . We have

$$\frac{1}{\epsilon} = \frac{1}{\cos^{-1}(z_0)} = \frac{1}{\cos^{-1}\left(1 - \left(\frac{2}{(1-a)^2} - 2\right)k^{-2} + O(k^{-4})\right)}. \tag{104}$$

By Puiseux expansion,  $\cos^{-1}(1-x)$  is

$$\cos^{-1}(1-x) = \sqrt{2x} + O(x^{\frac{3}{2}}). \tag{105}$$

It follows that

$$\begin{aligned}
\frac{1}{\epsilon} &= \frac{1}{\cos^{-1}(1 - \left(\frac{2}{(1-a)^2} - 2\right)k^{-2} + O(k^{-4}))} \\
&= \frac{1}{\sqrt{2\left(\frac{2}{(1-a)^2} - 2\right)k^{-2} + O(k^{-4})} + O(k^{-2})^{\frac{3}{2}}} \\
&= \frac{k}{\sqrt{2\left(\frac{2}{(1-a)^2} - 2\right)(1 + O(k^{-2})) + O(k^{-2})}} \\
&= \frac{k}{\sqrt{2\left(\frac{2}{(1-a)^2} - 2\right)}} \cdot \frac{1}{1 + O(k^{-2})} \\
&= \frac{k}{\sqrt{2\left(\frac{2}{(1-a)^2} - 2\right)}} (1 + O(k^{-2})) \\
&= \frac{1-a}{2\sqrt{2a-a^2}} k (1 + O(k^{-2})). \tag{106}
\end{aligned}$$

Hence, we have proven that the reciprocal of angular precision, i.e.,  $\frac{1}{\epsilon}$ , is asymptotically linear to  $k$ , and the asymptote is  $\frac{1-a}{2\sqrt{2a-a^2}} k$  that  $\frac{1}{\epsilon}$  trends when  $k \rightarrow \infty$ .

## Appendix L. Special form of ACG distribution inference

In this section, we prove that the iterative method for determining the maximum-likelihood approximation of  $k$  in the special-form ACG distribution covariance matrix  $\mathbf{A}$  holds. We denote  $k^2$  by  $\xi$ , and  $\bar{\mathbf{q}}^{-1} \otimes \mathbf{q}_i$  by  $\begin{pmatrix} q_{0i} \\ \mathbf{n}_{\mathbf{q}_i} \end{pmatrix}$ . We adapt the method in Tyler (1987) to determine the maximum-likelihood estimate of the parameter  $k$  for  $ACG(\mathbf{A})$ , where  $\mathbf{A} = \begin{pmatrix} k^2 & & \\ & 1 & \\ & & 1 \end{pmatrix}$ . The likelihood function for  $\xi$  is

$$\begin{aligned}
L(\xi) &:= \xi^{-\frac{N}{2}} \sum_{i=1}^N ((\bar{\mathbf{q}}^{-1} \otimes \mathbf{q}_i)^T \hat{\mathbf{A}}^{-1} (\bar{\mathbf{q}}^{-1} \otimes \mathbf{q}_i))^{-2} \\
&= \xi^{-\frac{N}{2}} \sum_{i=1}^N (\xi^{-1} q_{0i}^2 + \mathbf{n}_{\mathbf{q}_i} \cdot \mathbf{n}_{\mathbf{q}_i})^{-2}. \tag{107}
\end{aligned}$$

The maximum-likelihood estimate  $\xi$  satisfies

$$\begin{aligned}
\frac{d \log L(\xi)}{d \xi} &= 0 \\
\Rightarrow -\frac{N}{2\xi} - 2 \sum_{i=1}^N \frac{-\xi^{-2} q_{0i}^2}{\xi^{-1} q_{0i}^2 + \mathbf{n}_{\mathbf{q}_i} \cdot \mathbf{n}_{\mathbf{q}_i}} &= 0 \\
\Rightarrow \xi &= \frac{4}{N} \sum_{i=1}^N \frac{q_{0i}^2}{\xi^{-1} q_{0i}^2 + \mathbf{n}_{\mathbf{q}_i} \cdot \mathbf{n}_{\mathbf{q}_i}}, \tag{108}
\end{aligned}$$

where  $\xi = k^2$ . Thus, we have proven that Eq. (41) is an iteration formula for solving  $k$ .

## References

- Baldwin, P.R., Penczek, Paweł A., 2007. The transform class in sparx and eman2. *Journal of Structural Biology* 157 (1), 250–261.
- Bazett-Jones, David P., Mendez, Elizabeth, Czarnota, Gregory J., Peter Ottensmeyer, F., Allfrey, Vincent G., 1996. Visualization and analysis of unfolded nucleosomes associated with transcribing chromatin. *Nucleic Acids Research* 24 (2), 321–329.
- Berthold Horn. Closed-form solution of absolute orientation using unit quaternions. *Journal of the Optical Society of America A* 4, 629–642, 04 1987.
- Conway John H., Smith Derek A., 2003. On Quaternions and Octonions, first ed.
- Coxeter, Harold Scott Macdonald, 1973. Regular polytopes. Courier Corporation.
- Czarnota, Gregory J., Ottensmeyer, F.P., 1996. Structural states of the nucleosome. *Journal of Biological Chemistry* 271 (7), 3677–3683.
- Czarnota, Gregory J., Andrews, David W., Farrow, Neil A., Ottensmeyer, F.P., 1994. A structure for the signal sequence binding protein srp54: 3d reconstruction from stem images of single molecules. *Journal of Structural Biology* 113 (1), 35–46.
- Przemysław Dobrowolski, 2015. Swing-twist decomposition in clifford algebra. arXiv e-prints, page arXiv:1506.05481.
- Prakash Dube, Elena V Orlova, Friederich Zemlin, Marin van Heel, J. Robin Harris, Jurgen Markl, 1995. Three-dimensional structure of keyhole limpet hemocyanin by cryo-electron microscopy and angular reconstitution. *Journal of Structural Biology* 115 (3) 226–232.
- Farrow, Neil A., Ottensmeyer, E. Peter, 1992. A posteriori determination of relative projection directions of arbitrarily oriented macromolecules. *JOSA A* 9 (10), 1749–1760.
- Farrow, Neil A., Peter Ottensmeyer, F., 1993. Automatic 3d alignment of projection images of randomly oriented objects. *Ultramicroscopy* 52 (2), 141–156.
- Frank, Joachim, Radermacher, Michael, Penczek, Paweł, Zhu, Jun, Li, Yanhong, Ladadj, Mahieddine, Leith, Ardean, 1996. Spider and web: processing and visualization of images in 3d electron microscopy and related fields. *Journal of Structural Biology* 116 (1), 190–199.
- Georgy Derevyanko, Guillaume Lamoureux, 2018. Torchproteinlibrary: A computationally efficient, differentiable representation of protein structure. arXiv preprint arXiv:1812.01108.
- Grant, Timothy, Rohou, Alexis, Grigorieff, Nikolaus, 2018. cistem: User-friendly software for single-particle image processing 7 (a2) C1368–C1368.
- Grigorieff, Nikolaus, 2018. Frealign: High-resolution refinement of single particle structures 157 (1), 0–125.
- Tang, Guang, Peng, Liwei, Baldwin, Philip R., Mann, Deepinder S., Jiang, Wen, Rees, Ian, Ludtke, Steven J., 2007. Eman2: An extensible image processing suite for electron microscopy 157 (1), 0–46.
- Gurski, K.M., Hivon, E., Banday, A.J., Wandelt, B.D., Hansen, F.K., Reinecke, M., Bartelmann, M., 2005. Healpix: a framework for high-resolution discretization and fast analysis of data distributed on the sphere. *The Astrophysical Journal* 622 (2), 759–771.
- Gydo Cp van Zundert, Alexandre Mjj Bonvin, 2015. Fast and sensitive rigid-body fitting into cryo-em density maps with powerfit. *AIMS Biophysics* 2(2), 73–87.
- William Rowan Hamilton, 1844. On a new species of imaginary quantities connected with a theory of quaternions. In: Proceedings of the Royal Irish Academy, vol. 2, pp. 4–1.
- Harauz, George, 1990. Representation of rotations by unit quaternions. *Ultramicroscopy* 33 (3), 209–213.
- Herman, Gabor T., Frank, Joachim, 2014. *Computational Methods for Three-Dimensional Microscopy Reconstruction*. Springer.
- Horn Roger A., 1985. Matrix analysis, Cambridge: Cambridge University Press, Cambridge.
- Brabe, Thomas, 2015. Localize.pytom: a modern webserver for cryo-electron tomography. *Nucleic Acids Research* 43 (W1), W231–W236.
- Du, Huynh, 2009. Metrics for 3d rotations: Comparison and analysis. *Journal of Mathematical Imaging and Vision* 35 (2), 155–164.
- Irina I. Serysheva, Elena V. Orlova, Wah Chiu, Michael B. Sherman, Susan L. Hamilton, Marin Van Heel, 1995. Electron cryomicroscopy and angular reconstitution used to visualize the skeletal muscle calcium release channel. *Nature Structural Biology* 2 (1), 18–24.
- Jacques, Ian, 1987. *Numerical Analysis*. Springer, Netherlands, Dordrecht.

- Frank, Joachim, Shimkin, Brian, Dowse, Helen, 1981. Spider—a modular software system for electron image processing. *Ultramicroscopy* 6 (1), 343–357.
- Karney, Charles F.F., 2007. Quaternions in molecular modeling. *Journal of Molecular Graphics and Modelling* 25 (5), 595–604.
- Kuffner James J., 2004. Effective sampling and distance metrics for 3d rigid body path planning. In: IEEE International Conference on Robotics and Automation, 2004. Proceedings. ICRA'04. 2004, IEEE, vol. 4, pp. 3993–3998.
- Kuo, John, 2007. *Electron Microscopy: Methods and Protocols*, vol. 369 Springer Science & Business Media.
- Leon Steven J., 1986. Linear algebra with applications, New York: Macmillan, New York, second ed.
- Liu, Xiangan, Jiang, Wen, Jakana, Joanita, Chiu, Wah., 2007. Averaging tens to hundreds of icosahedral particle images to resolve protein secondary structure elements using a multi-path simulated annealing optimization algorithm. *Journal of Structural Biology* 160 (1), 11–27.
- Mardia, K.V., 2000. Directional statistics. Chichester; New York: Wiley, Chichester; New York, second ed.
- Mingxu, Hu, Hongkun, Yu, Kai, Gu, Wang, Zhao, Ruan, Huabin, Wang, Kunpeng, Ren, Siyuan, Li, Bing, Gan, Lin, Shizhen, Xu, Yang, Guangwen, Shen, Yuan, Li, Xueming, 2018. A particle-filter framework for robust cryo-em 3d reconstruction. *Nature Methods* 15 (12), 1083–1089.
- Moakher, Maher, 2002. Means and averaging in the group of rotations. *SIAM Journal on Matrix Analysis and Applications* 24 (1), 1–16.
- Nachbin, Leopoldo, 1965. The Haar Integral, Princeton, N.J.: D. Van Nostrand Co., Inc., Princeton, N.J.
- E.V. Orlova, M. Van Heel, 1994. Angular reconstitution of macromolecules with arbitrary point-group symmetry. In: Jouffrey, B., Colliex, C. (Eds). Proc 13th Intern Congress Electron Microsc. Les Editions de Physique, Les Ulis, vol. 1, pp. 507–508.
- Orlova, Elena V., Serysheva, Irina I., van Heel, Marin, Hamilton, Susan L., Chiu, Wah., 1996. Two structural configurations of the skeletal muscle calcium release channel. *Nature Structural Biology* 3 (6), 547–552.
- Orlova Elena V., Prakash Dube, Robin Harris, J., Erich Beckman, Friedrich Zemlin, Jurgen Markl, Marin van Heel, 1997. Structure of keyhole limpet hemocyanin type 1 (klh1) at 15 Å resolution by electron cryomicroscopy and angular reconstitution. *Journal of Molecular Biology* 271 (3) 417–437.
- Yaakov Oshman, Markley, F., Yang Cheng, Crassidis John L., 2007. Quaternion averaging. Oshman, Yaakov, Carmi, Avishy, 2006. Attitude estimation from vector observations using a genetic-algorithm-embedded quaternion particle filter. *Journal of Guidance, Control, and Dynamics* 29 (4), 879–891.
- Arun Prasad Pandurangan, Daven Vasishtan, Frank Alber, Maya Topf, 2015. r-tempy: simultaneous fitting of components in 3d-em maps of their assembly using a genetic algorithm. *Structure* 23 (12), 2365–2376.
- Plaisier, J.R., Jiang, L., Abrahams, J.P., 2007. Cyclops: New modular software suite for cryo-em. *Journal of Structural Biology* 157 (1), 19–27.
- Punjani, Ali, Rubinstein, John L., Fleet, David J., Brubaker, Marcus A., 2017. cryosparc: algorithms for rapid unsupervised cryo-em structure determination. (cryo-electron microscopy single-particle ab initio reconstruction and classification)(report). *Nature Methods* 14(3):290.
- Schatz, Michael, Orlova, Elena V., Dube, Prakash, Juger, Joachim, van Heel, Marin, 1995. Structure of *lumbricus terrestris* hemoglobin at 30 Å resolution determined using angular reconstitution. *Journal of Structural Biology* 114 (1), 28–40.
- Michael Schatz, Orlova, E.V., Dube, P., Stark, H., Zemlin, F., Van Heel, M., 1997. Angular reconstitution in three-dimensional electron microscopy: Practical and technical aspects. *Scanning Microscopy* 11, 179–193.
- Scheres, Sjors H.W., 2012. Relion: Implementation of a bayesian approach to cryo-em structure determination. *Journal of Structural Biology* 180 (3), 519–530.
- Saikh, Tanvir R., Gao, Haixiao, Baxter, William T., Asturias, Francisco J., Boisset, Nicolas, Leith, Ardean, Frank, Joachim, 2008. Spider image processing for single-particle reconstruction of biological macromolecules from electron micrographs. 3 (12), 1941–1974.
- Slama, Chester C., 1980. Manual of photogrammetry. Technical report, America Society of Photogrammetry.
- Sommer, Ingolf, Brimacombe, Richard, 2001. Methods for refining interactively established models of ribosomal rna towards a physico-chemically plausible structure. *Journal of Computational Chemistry* 22 (4), 407–417.
- Srivastava, Anuj, Klassen, Eric P., 2016. *Functional and Shape Data Analysis*. Springer, New York, New York, NY, New York, NY.
- Holger Stark, Florian Mueller, Elena V. Orlova, Michael Schatz, Prakash Dube, Tarik Erdemir, Friedrich Zemlin, Richard Brimacombe, Marin van Heel, 1995. The 70s *escherichia coli* ribosome at 23 Å resolution: fitting the ribosomal rna. *Structure* 3 (8), 815–821.
- Holger Stark, Elena V. Orlova, Jutta Rinke-Appel, Nicole Junke, Florian Mueller, Marina Rodnina, Wolfgang Wintermeyer, Richard Brimacombe, Marin van Heel, 1997. Arrangement of trnas in pre-and posttranslocational ribosomes revealed by electron cryomicroscopy. *Cell* 88 (1), 19–28.
- John Stillwell, 2008. *Naive Lie Theory*. New York, NY: Springer New York, New York, NY.
- Topf, Maya, Lasker, Keren, Webb, Ben, Wolfson, Haim, Chiu, Wah., Sali, Andrej, 2008. Protein structure fitting and refinement guided by cryo-em density. *Structure* 16 (2), 295–307.
- Tyler, David E., 1987. Statistical analysis for the angular central gaussian distribution on the sphere. *Biometrika* 74 (3), 579–589.
- Vince, John, 2011. *Quaternions for Computer Graphics*. Springer, London, London, London.
- Wasilewski, Sebastian, Rosenthal, Peter B., 2014. Web server for tilt-pair validation of single particle maps from electron cryomicroscopy. *Journal of Structural Biology* 186 (1), 122–131.
- Winitzki, Sergei, 2010. *Linear algebra via exterior products*. Sergei Winitzki.
- Anna Yershova, Swati Jain, Steven M. Lavalle, Julie C. Mitchell, 2010. Generating uniform incremental grids on so(3) using the hopf fibration. *The International Journal of Robotics Research* 29 (7) 801–812.